

# Multimodal Connectivity-Based Parcellation Reveals a Shell-Core Dichotomy of the Human Nucleus Accumbens

Xiaoluan Xia,<sup>1</sup> Lingzhong Fan,<sup>2</sup> Chen Cheng,<sup>1</sup> Simon B. Eickhoff,<sup>4,5</sup>  
Junjie Chen,<sup>1</sup> Haifang Li,<sup>1\*</sup> and Tianzi Jiang<sup>2,3,6,7\*</sup>

<sup>1</sup>College of Computer Science and Technology, Taiyuan University of Technology, Taiyuan 030600, China

<sup>2</sup>Brainnetome Center, Institute of Automation, Chinese Academy of Sciences, Beijing 100190, China

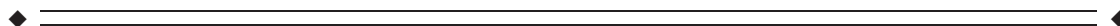
<sup>3</sup>National Laboratory of Pattern Recognition, Institute of Automation, Chinese Academy of Sciences, Beijing 100190, China

<sup>4</sup>Institute of Neuroscience and Medicine (INM-1), Research Centre Juelich, 52425 Juelich, Germany

<sup>5</sup>Institute for Clinical Neuroscience and Medical Psychology, Heinrich-Heine-University Düsseldorf, Düsseldorf 40225, Germany

<sup>6</sup>CAS Center for Excellence in Brain Science and Intelligence Technology, Institute of Automation, Chinese Academy of Sciences, Beijing 100190, China

<sup>7</sup>The Queensland Brain Institute, University of Queensland, Brisbane, QLD, 4072, Australia



**Abstract:** The subdifferentiation of the nucleus accumbens (NAc) has been extensively studied using neuroanatomy and histochemistry, yielding a well-accepted dichotomic shell/core architecture that reflects dissociable roles, such as in reward and aversion, respectively. However, in vivo parcellation of these structures in humans has been rare, potentially impairing future research into the structural and functional characteristics and alterations of putative NAc subregions. Here, we used three complementary parcellation schemes based on tractography, task-independent functional connectivity, and task-dependent co-activation to investigate the regional differentiation within the NAc. We found that a 2-cluster solution with shell-like and core-like subdivisions provided the best description of the data and was consistent with the earlier anatomical shell/core architecture. The consensus clusters from

Additional Supporting Information may be found in the online version of this article.

Xiaoluan Xia and Lingzhong Fan Co-first author.

Contract grant sponsor: National Key Basic Research and Development Program (973); Contract grant numbers: 2011CB707801 and 2012CB720702; Contract grant sponsor: Strategic Priority Research Program of the Chinese Academy of Sciences; Contract grant number: XDB02030300; Contract grant sponsor: Natural Science Foundation of China; Contract grant numbers: 91432302, 91132301, 81501179, 81270020, 61373101, 61472270, and 61402318; Contract grant sponsor: Deutsche Forschungsgemeinschaft; Contract grant number: DFG, EI 816/4-1; EI 816/6-1; Contract grant sponsor: National Institute of Mental Health; Contract grant number: R01-MH074457; Contract grant sponsor: Helmholtz Portfolio Theme “Supercomputing and Modeling for the Human Brain”

and the European Union Seventh Framework Programme; Contract grant number: 604102; Contract grant sponsor: Beijing Municipal Science & Technology Commission; Contract grant number: Z161100000216139.

\*Correspondence to: Haifang Li, College of Computer Science and Technology, Taiyuan University of Technology, Taiyuan 030600, China. E-mail: lihaifang@tyut.edu.cn or Tianzi Jiang, Brainnetome Center, Institute of Automation, Chinese Academy of Sciences, Beijing 100190, China. E-mail: jiangtz@nlpr.ia.ac.cn

Received for publication 27 September 2016; Revised 14 April 2017; Accepted 21 April 2017.

DOI: 10.1002/hbm.23636

Published online 26 May 2017 in Wiley Online Library (wileyonlinelibrary.com).

this optimal solution, which was based on the three schemes, were used as the final parcels for the subsequent connection analyses. The resulting connectivity patterns presented inter-hemispheric symmetry, convergence and divergence across the modalities, and, most importantly, clearly distinct patterns between the two subregions. This convergent connectivity patterns also confirmed the connections in animal models, supporting views that the two subregions could have antagonistic roles in some circumstances. Finally, the identified parcels should be helpful in further neuroimaging studies of the NAc. *Hum Brain Mapp* 38:3878–3898, 2017. © 2017 Wiley Periodicals, Inc.

**Key words:** nucleus accumbens; connectivity-based parcellation; tractography; functional connectivity; meta-analytic connectivity modeling

## INTRODUCTION

The nucleus accumbens (NAc) of the human brain, located ventral and slightly medial to the head of the caudate nucleus, forms an integral part of the ventral striatum. Although clear-cut borders have only been partially identified [Cauda et al., 2011; Voorn et al., 2004], it has been accepted as an integral, but specialized, part of the striatal complex [Heimer et al., 1991]. The NAc plays a pivotal role in refining action selection [for review, see Floresco, 2015] and has been an important target for deep brain stimulation (DBS) and novel biological therapies in anxiety- and obsessive-compulsive disorders, for example, depression and addiction [for review, see Blomstedt et al., 2013; Gelfand and Kaplitt, 2013; Sturm et al., 2003].

Numerous studies further confirmed multiaspect heterogeneity of the NAc, resulting in various parcellation schemes based on this multiaspect heterogeneity [for review, see Salgado and Kaplitt, 2015]. Zaborszky et al. [1985] first parcellated rodent NAc into shell and core based on a differential distribution of cholecystokinin immunoreactivity, with the latter being more medial and ventral than the former. This dichotomy was subsequently established using various schemes in monkeys [Brauer et al., 2000] and humans [Groenewegen et al., 1996]. Another important parcellation, a mosaic arrangement of patches and matrix, particularly in the core subregion, was defined by the conjunction of histochemical markers together with intrinsic inputs-outputs in studies at a finer neuronal circuit level [Arts and Groenewegen, 1992; Humphries and Prescott, 2010]. In addition to these common solutions, the shell was further subdivided into medial and lateral areas, or even more subregions, based on their unique sets of inputs and outputs [Ikemoto, 2007]. The rostral pole was identified because of its specific efferent projections in rodents [Zahm and Brog, 1992; Zahm and Heimer, 1993] but not in primates [Ikemoto et al., 1995; McCollum and Roberts, 2014]. Although multiple levels of complex organization have been identified, to date the shell-core dichotomy has been the most intensely investigated. However, the aforementioned studies almost entirely utilized traditional anatomic or histochemical techniques. In human neuroimaging, the NAc or area

containing the NAc was separated from the striatum by some researchers but without a further subdivided [Draganski et al., 2008; Fan et al., 2016; Janssen et al., 2015; Tziortzi et al., 2013]. For NAc-specific parcellation, Baliki et al. [2013] used a tractography-based approach to parcellate the human right NAc into pshell and pcore subregions, roughly corresponding to the anatomical shell and core, respectively, at a coarse-grained level.

Key insights into the specific functions of the NAc subregions were gained in numerous lesion, stimulation, and neural recording studies conducted in animal models [for review, see Nicola, 2007]. Additionally, the neural substrates underlying these functions have been further investigated [Reed et al., 2015; for review, see Basar et al., 2010; Salgado and Kaplitt, 2015]. The shell and core were each found to be functionally aimed at facilitating the selection of the best available reward, but promoted distinct patterns of behavior [cf. Floresco, 2015]. The shell receives prominent projections from the ventromedial prefrontal cortex [Heidbreder and Groenewegen, 2003], hippocampus (HIPP) [Groenewegen et al., 1987], amygdala (AMYG) [Wright and Groenewegen, 1996], the small, but important, projections from the thalamic subregions of the intralaminar and midline nuclei [Van der Werf et al., 2002], as well as dopamine (DA) from the ventral tegmental area (VTA) [Stopper and Floresco, 2011]. Functionally, the shell plays a role in suppressing less- or non-rewards stimuli that may interfere with the association with the best available reward-predicting stimuli, by way of value-driven decision making. The core, however, receives prominent projections from the anterior cingulate cortex (ACC) [Parkinson et al., 2000], intralaminar and midline nuclei [Van der Werf et al., 2002; Zhu et al., 2016], anterior part of the basolateral amygdala [Cardinal and Everitt, 2004], and DA from the substantia nigra (SN) [Bjorklund and Dunnett, 2007]. Functionally, the core plays a role in selectively instigating an approach toward an incentive stimulus associated with the best available reward after Pavlovian cue encoding. In addition, more accurate, anatomically localized studies suggested that the NAc shell and core play prominent roles in reward [Castro and Berridge, 2014; Pecina and Berridge, 2005] and aversion [Castro et al., 2016; Yamaguchi et al., 2015] processing, respectively. DBS of the NAc

shell and core also resulted in opposite effects on impulsive action [Sesia et al., 2008]. However, these findings about the subregions from animal studies have not yet been well-documented in in vivo human imaging. Baliki et al. [2013] exhibited distinct connectivity profiles for the pshell and pcore subregions but they were not well-characterized across modalities; while another investigator deliberately constructed the subregions as having regularly shaped volumes [Aharon et al., 2006] based on previous anatomical information. All these studies support the dissociable roles of the NAc subregions to some degree.

In addition to the commonly used connectivity-based parcellation (CBP) [Eickhoff et al., 2015], highly structured brain spontaneous fluctuations [Deco et al., 2013], that result in types that are distinct but have closely related connectivity patterns have been utilized to parcellate brain regions into consensus subregions across modalities [Bzdok et al., 2013; Wang et al., 2015]. Previous researchers have identified highly consistent distributions of parcels in the optimal solutions for different brain areas [Genon et al., 2017; Kelly et al., 2012]. These studies found convergent as well as divergent connectivity characteristics across subregions and/or modalities without any additional comparisons of the connectivity patterns. Whether consensus subregions exist in the NAc and their connective characteristics across hemispheres, modalities, and subregions needed to be explored.

To address these issues, three CBP schemes based on probabilistic diffusion tractography (PDT-CBP) [Fan et al., 2016], resting-state functional connectivity (rsFC-CBP) [Wang et al., 2016], and meta-analytic connectivity modeling (MACM-CBP) [Ray et al., 2015] were used to parcellate the NAc. For the former two schemes, we used high-quality MRI data from the Human Connectome Project (HCP) [Sotiropoulos et al., 2013; Van Essen et al., 2013] and applied mixed registration methods. The latter two schemes were used on these nuclei for the first time, as far as we know. The consensus clusters across the three schemes were utilized in the subsequent connection analyses from whole-brain voxel-wise and connectivity fingerprints perspectives. We further compared the connectivity patterns across the hemispheres, modalities, and subregions [cf. Mars et al., 2016] and investigated the dissociable roles of the subregions supported by their characteristic connectivity patterns.

## MATERIALS AND METHODS

### Subjects and MRI Acquisition

#### Subjects

(1) We first randomly extracted 80 subjects from the HCP to test the accuracy of a new local registration method, NABC (cf. Supporting Information Methods I.2), and the definition of the region of interest (ROI). (2) Misregistration may impact parcellation quality (cf. Supporting

Information Limitations and improvements). Therefore, to lessen this impact, we selected the 40 subjects (ages 22–35; 22 males) who had the highest Dice coefficients [Dice, 1945] out of the HCP-80 for the registration accuracy and used them to increase the accuracy of the parcellation. This HCP-40 dataset has sufficient statistical power for subsequent characterization of the connectivity patterns of the subregions.

#### MRI acquisition

All of the experimental data extracted from the HCP were obtained on a customized 3T Siemens Skyra using a 32-channel head coil [cf. Van Essen et al., 2013]. The data included high-resolution T1/T2-weighted structural MRI (sMRI) [Ugurbil et al., 2013] data acquired using a 3D MPRAGE sequence with 0.7 mm isotropic resolution; diffusion MRI (dMRI) [Sotiropoulos et al., 2013; Ugurbil et al., 2013] data acquired using a multishell approach at a 1.25 mm isotropic resolution; and resting-state fMRI (rs-fMRI) [Smith et al., 2013; Ugurbil et al., 2013] data acquired while the participants relaxed with their eyes open, using a gradient echo planar imaging (EPI) sequence with 2 mm isotropic resolution, and 1,200 time points. In this current study, we only chose the first run of the rs-fMRI, which took about 14.5 min per subject. Finally, we used the preprocessed sMRI data, according to the HCP minimal processing pipelines (Supporting Information Methods I.1) for the image registration and definition of the ROI.

#### Mixed Registration Methods

When registering a small brain region, such as the NAc, between individuals, the traditional nonlinear registration method may impair the registration accuracy, limiting the parcellation quality. We generalized a locally weighted registration method of the automated brainstem co-registration method [Napadow et al., 2006] to the NAc, and termed it NAc-based co-registration (NABC; detailed in Supporting Information Methods I.2). The HCP-80 group was employed to identify differences between the NABC and the common-used nonlinear registration, FSL/FNIRT [Jenkinson et al., 2012] via a paired-samples *t*-test. The results showed that the NABC (Fig. 1; LH:  $0.845 \pm 0.035$ ; RH:  $0.833 \pm 0.035$ ,  $\mu \pm \sigma$ ) had significantly greater registration accuracy than the FNIRT (left:  $0.813 \pm 0.038$ , at  $P < 10^{-6}$ ; right:  $0.814 \pm 0.040$ , at  $P < 10^{-4}$ ). Therefore, for the subsequent registrations of the local brain images limited to the NAc, we chose the NABC method. But for the registrations of the whole-brain distributed images, NABC had a low accuracy, so we used FNIRT. To register the images between modalities within an individual, we used a customized 6 degrees of freedom (DOF) FLIRT BBR + BBRegister algorithm [Glasser et al., 2013].

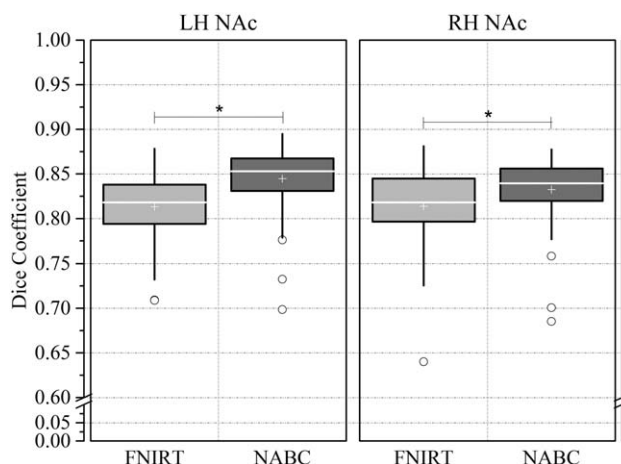


**Figure 1.**

Comparisons between FNIRT and NABC. Box and whisker plots show the Dice (registration accuracy) between the deformed source and the target label volumes and then the average across brain pairs. Box lines at the lower quartile, median and upper quartile values, and whiskers extend from each end of the box to 1.5 times the interquartile range. Outliers were indicated by “o.” A paired samples *t*-test tested the differences between the two methods ( $*P < 10^{-4}$ ). LH: left hemisphere; RH: right hemisphere.

### Definition of the ROI

For each subject in the HCP-80, we extracted a rough NAc mask from their T1w image using FSL’s FIRST [Patenaude et al., 2011]. We then used the T2w (or T1w divided by T2w) image as the background because of its enhanced contrast between the NAc and caudate-putamen (CPU) [Mavridis et al., 2011] compared with the T1w image [Neto et al., 2008] and overlaid it with the rough NAc mask, manually correcting any obvious departures by referring to well-accepted structural conventions of the NAc based on anatomical landmarks [Breiter et al., 2001] (<http://www.cma.mgh.harvard.edu/manuals/segmentation/>). Then, all the individual specific NAc maps were transformed into standard (MNI) space using NABC to create a group-averaged NAc map. The final ROI was generated by thresholding the group-averaged NAc map at  $>70\%$  probability and performing a subsequent binary conversion (Supporting Information Fig. S1. left NAc:  $876 \text{ mm}^3$  and right NAc:  $800 \text{ mm}^3$ ).

### Data Preprocessing

For each subject in the HCP-40 dataset, we used the pre-processed dMRI and fMRI data in whole and in part, respectively, according to the HCP minimal processing pipelines (cf. Supporting Information Methods I.3, I.4).

We segmented their preprocessed T1w images into different tissue types using FSL’s FAST [Zhang et al., 2001].

The gray matter (GM), white matter (WM), and cerebrospinal fluid (CSF) masks were brought into subject-native function and diffusion space for further analyses, such as nuisance covariates regression. In addition, the GM masks were transformed into standard MNI space using FNIRT to calculate the group-averaged GM mask (thresholded at  $>0.5$ ) primarily for use in the group-level statistical analysis.

The preprocessed dMRI data were used to estimate the fiber orientations and the uncertainty using FSL’s multi-shell spherical deconvolution toolbox “bedpostx” [Jbabdi et al., 2012]. The number of fiber compartments in each voxel was determined using automatic relevance determination priors [Behrens et al., 2007].

We analyzed the rs-fMRI data using FSL and custom-made software written in MATLAB. Transforming functional data between subject-native and standard MNI space can introduce large, wide-spread effects on rs-fMRI correlations due to imperfect registration [Seibert and Brewer, 2011], so we preprocessed the “unprocessed” HCP rs-fMRI data in subject-native space (cf. Supporting Information Methods I.4). Note that we regressed out the confounding head movement time series (six motion parameters) and the mean time series of the WM and CSF. To spatially smooth the data, we used a 6 mm Gaussian kernel of FWHM. Additionally, to reduce the low-frequency drift and high-frequency noise, a band-pass filter was used to separate the data at slow-4 (0.027–0.073 Hz), which is known to have higher amplitudes in many brain regions including the basal ganglia, thalamus, and CPU [Zuo et al., 2010].

### Connectivity-Based Parcellation

#### PDT-CBP

The final ROI in standard MNI space was brought back into subject-native structural space using NABC and then back into diffusion space using the 6 DOF FLIRT BBR + BBRegister masked by the GM mask in subject-diffusion space to remove a very limited number of voxels misregistered into the WM/CSF. Subsequently, whole-brain probabilistic streamline tractography was implemented for each voxel in the seed mask, and the connection and cross-correlation matrixes [Johansen-Berg et al., 2004] were constructed for this seed mask in subject-native diffusion space. The latter was further fed into spectral clustering, which automatically subdivided all the voxels in the seed mask into multiple subgroups [Baldassano et al., 2015]. Then, voxels in every subgroup were mapped back onto the brain to generate the subregions in diffusion space (detailed in Supporting Information Methods I.3).

Note that one open issue with the spectral clustering algorithm is the number of clusters, which need to be set by the investigator beforehand. In this study, we set it to range from 2 to 4 (cf. Discussion). Subsequently, every parcellation result was transformed into standard MNI



space via a subject-native structural scan using NABC. Group-level probability maps of the subregions, reflecting the inter-individual variability of each given subregion [Caspers et al., 2008], were created by overlapping the corresponding subregions for all the subjects in MNI space; then the group-overlapped subregions maps were thresholded at >50% probability to generate the final subregions' binarized mask for each solution.

### rsFC-CBP

Using a procedure (detailed in Supporting Information Methods I.4) that was similar to PDT-CBP, the seed mask was transformed into subject-native function space for every subject and masked by the GM mask in subject-function space. We calculated the whole-GM resting-state functional connectivity (rsFC) for each voxel in the seed mask and constructed the similarity matrix based on every possible pair of rsFC maps using  $\eta^2$ , which can provide a better measure of the similarity between rsFC maps than does a spatial correlation [Cohen et al., 2008; Kelly et al., 2010]. The resulting  $\eta^2$  matrix is similar to the cross-correlation matrix obtained in PDT-CBP.

$$\eta^2 = 1 - \frac{SS_{\text{within}}}{SS_{\text{combined}}} = 1 - \frac{\sum_{i=1}^n (a_i - m_i)^2 + (b_i - m_i)^2}{\sum_{i=1}^n (a_i - \bar{M})^2 + (b_i - \bar{M})^2}$$

where,  $a_i$  and  $b_i$  are values at position  $i$  in the iFC maps of  $a$  and  $b$  respectively;  $m_i$  is the mean value of the two iFC maps at position  $i$ ; and  $\bar{M}$  is the grand mean across all locations in both correlation maps.

The  $\eta^2$  matrix was then fed into spectral clustering, which automatically subdivided these voxels into subgroups that were preset to 2–4. Then each subgroup's voxels were separately mapped back onto the brain as the individual NAc subregions in function space. Each individual result was transformed into standard MNI space via a subject-native structural scan to generate a group-level subdivisions' probability map and to obtain the final subregions' binarized mask for each solution by thresholding the group-overlap subregions at >50% probability. The parcellation parameters were consistent with PDT-CBP for comparison purposes.

### MACM-CBP

We used the MACM package [Eickhoff et al., 2011; Robinson et al., 2010] in the MATLAB environment to perform a task-dependent co-activation-based parcellation. The MACM13 version provided 7,377 functional neuroimaging experiments (67,620 foci) for the whole-brain mask after searching the BrainMap database [Laird et al., 2009] (<http://www.brainmap.org/>) with the following constraints: (i) only fMRI and PET experiments; (ii) normal mapping in stereotaxic coordinates; and (iii) healthy adults.

For each voxel in the NAc seed mask in standard MNI space, we selected the nearest 20, 22, 24 ... or 100 sets of

experiments that reported the closest activation to a given seed voxel (i.e., 41 filter sizes). For each filter size, these selected experiments, in which all the foci were processed by 3D Gaussian probability distributions and then combined into a modeled activation map (MA), were used to calculate the brain-wide activation likelihood estimation score (ALE) for the given voxel [Eickhoff et al., 2012; Turkeltaub et al., 2012]. These ALE scores were not thresholded so that they would retain the complete pattern of co-activation likelihood. All of the ALE scores that corresponded to the NAc voxels were combined into a co-activation map, yielding 41 voxel-wise brain-wide coactivation maps that corresponded to the 41 different filter sizes. These coactivation maps were then fed into  $k$ -means clustering separately with the  $k$  preset from 2 to 4, that is, the same number as was used for the PDT-CBP and rsFC-CBP, yielding 3 (number of clusters)  $\times$  41 (filter size) independent cluster solutions. Finally, we determined the most stable range of filter sizes, that is, those that produced solutions that were most similar to the consensus solution, as well as the optimal parcellation solution.

### Determining the Optimal Parcellation Solution and the Consensus Clusters

We used the spectral clustering algorithm (for PDT-CBP and rsFC-CBP) and the  $k$ -means algorithm (for MACM-CBP). The clusters number,  $k$ , of these algorithms was set from 2 to 4. To choose the optimal clusters, that is, the parcel numbers, we used two metrics (cf. Supporting Information Methods I.5). The Dice was used to assess the inter-individual, inter-scheme consistency for a subregion, and the variation of information (VI) [Meilă, 2007], which can be used to quantify the dissimilarity between two clustering solutions based on information-theory, was used to calculate a given  $k$  solution and its parent  $k - 1$  solution, as described elsewhere [Clos et al., 2013; Kelly et al., 2010]. Its solutions are considered stable if there is a significant increase in VI from the  $k$  (current) to the  $k + 1$  solution (primary criterion) or if there is a significant decrease from  $k - 1$  to the  $k$  solution (secondary criterion). The VI and the across-schemes mean of the VI were also used to identify the optimal solution.

After determining the optimal solution, the voxels that were consistently assigned across the three schemes were overlapped and their intersections, those that had similar connective characteristics, were extracted as the final consensus clusters to form a multimodal parcellation [Bzdok et al., 2013; Wang et al., 2015].

### Characterization of the Clusters: Whole-Brain Voxel-Wise Connectivity

To further characterize the anatomical connection (AC), rsFC, and coactivity profiles of the NAc subregions, the final consensus clusters were brought back into the subject-

native diffusion and function spaces of the selected 40 subjects.

## AC

In diffusion space, using a procedure that was similar to the procedure used for the PDT-CBP but for each subregion rather than for each voxel, 50,000 samples were drawn from the connectivity distribution to generate the whole-brain connectivity probability using the tool “probtrackx.” The connectivity probability was thresholded at  $>0.04\%$  of the samples [Fan et al., 2014] to reduce false positive connections. The identified fiber tracts were then binarized and transformed into standard MNI space. All the normalized fiber tracts across the subjects were averaged to obtain a probability fiber tracts map. The map was thresholded at 50% to generate the group-level common AC pattern for the given subregion.

## rsFC

A whole-brain rsFC map, the Pearson correlation coefficients between the mean time series for the given subregion, and the time series for each voxel in the GM mask were calculated in function space for each subject. All the rsFC maps were converted to  $z$ -values using Fisher’s  $z$ -transformation to improve normality and then transformed into standard MNI space. All these normalized  $z$ -valued rsFC maps were fed into a random effects one-sample  $t$ -test to determine the regions that had significant correlations with the NAc subregions in a voxel-wise manner. A statistical threshold of  $P$  (uncorrected)  $<0.001$  was set to achieve a corrected cluster-wise statistical significance of  $P < 0.05$ , with the cluster size estimated based on the group-averaged GM mask and the group-averaged Gaussian filter width. Further, minimum-statistic conjunction [Nichols et al., 2005] analyses were performed between all of the subregions, so that the surviving voxels had significant rsFC with all subregions. The extended threshold of the cluster size of the conjunction was set at 50. A contrasts rsFC was calculated using a paired samples  $t$ -test to compare the differences in the functional connection between all the pairs of the subregions. We set an uncorrected statistical threshold of  $P < 0.01$  to further achieve a corrected statistical significance of  $P < 0.05$  at the cluster-level.

## Coactivity

A follow-up MACM analysis was performed to characterize the coactivity profiles of these subregions in MNI space. Unlike the voxel-wise coactivation map aforementioned, a single ROI-wise map was created for each NAc subregion. Given a specific NAc subregion, all experiments in the BrainMap database that had at least one focus of activation close to this subregion, that is, any focus generalized by a specific 3D Gaussian probability distribution that overlapped with this subregion, was identified. Based

on these experiments, an ALE map was calculated and then compared to an ALE null distribution, which reflects a random spatial association between experiments with a fixed within-experiment distribution of foci [Eickhoff et al., 2009], to determine the regions that were significantly coactivated with the given subregion. Next, a nonparametric statistical image with  $P$ -values based on the proportion of equal or higher random values was generated by testing the observed ALE scores against the ALE scores obtained from the null-distribution from the random spatial association [Eickhoff et al., 2012]. This nonparametric  $P$ -values map was converted into  $z$ -scores and thresholded at a voxel-level  $P < 0.01$ . Then multiple comparisons were made using a cluster-level FWE-corrected threshold at  $P < 0.05$ . Similarly, a conjunction analysis was performed against the conjunction null hypothesis using the minimum statistic [Nichols et al., 2005]. The contrast analysis was performed to test the “true” difference between two MACMs against the contrast null-distribution with the resulting  $P$ -values thresholded at  $P < 0.95$  and an extended cluster threshold size of 50 [cf. Hoffstaedter et al., 2014].

We further assessed the degree of convergence between rsFC and MACM by performing the minimum-statistic for the conjunction analyses [Genon et al., 2017; Reid et al., 2016]. Only voxels with suprathreshold statistics for both the rsFC and MACM maps were included in the resulting conjunction, and the extended cluster threshold size was set at 50.

## Characterization of the Clusters: Fingerprints

Connectivity fingerprinting [Passingham et al., 2002] was employed to investigate the unique connectivity pattern of each cluster. The target areas were chosen from a combination of atlases, including the Harvard-Oxford probabilistic atlases covering both cortical and subcortical areas (thresholded at 50%) [Desikan et al., 2006], the Oxford thalamic connectivity atlas (thresholded at 50%) [Behrens et al., 2003], and the dopaminergic midbrain probabilistic atlas (thresholded at 50%) [Murty et al., 2014]. To identify the subcortical structures, we chose the caudate (Ca), putamen (Pu), pallidum (Pa), HIPPO, and AMYG from the Harvard-Oxford subcortical atlas, the thalamus from the finer-grained Oxford thalamic connectivity atlas, and the brainstem from the midbrain probabilistic atlas. The resulting combined atlas included 61 brain regions for each hemisphere.

For each specific NAc subregion and a specific connectivity type, a set of brain areas that met the criteria (cf. Supporting Information Methods I.6) were extracted to form a connectional family. The connectional values were normalized to the maximum connectional strength [Mars et al., 2012]. The tendency of the target areas to be connected to the NAc subregions, were calculated by the relative connections and then used to construct the fingerprint.

Because the prefrontal cortex has extensive and primary inputs to the NAc but the Harvard-Oxford atlas for

this area was relatively course-grained, we employed a finer-grained frontal atlas [Neubert et al., 2014] to detect the finer frontal connectivity pattern. The frontal atlas was created using PDT-CBP and subdivided the frontal and anterior cingulate cortices, yielding a total of 21 regions for each hemisphere. We investigated the specific frontal cortical AC with the NAc subregions using the same procedure.

### Comparisons Across Hemispheres, Modalities, and Subregions Using Fingerprints

Connectivity fingerprints have been extensively employed in comparative neuroscience to investigate the relationships between differences in the organization of different brains [cf. Mars et al., 2016]. We used it here to compare the connectivity patterns across hemispheres, modalities, and subregions. The target areas obtained using fingerprints from different modalities are sometimes inconsistent, but a unified organizational structure is necessary to compare these fingerprints. To avoid the risk of overfitting the fingerprint by having too many target areas [Mars et al., 2016], we used the intersections of the target areas across the modalities, the convergent fingerprint, for the comparisons across the modalities.

Finally, to ensure that any differences were not due to differences between the methods, all the comparisons were based on relative connectional values that were obtained using same methodology and parameters so that they only differed in their connections. Permutation tests were subsequently used to determine significant differences in the Manhattan distance between fingerprints, as described in Mars et al. [2016] (cf. Supporting Information Methods I.7), that is, to determine those that were lower (“close” relationship) or higher (“far” relationship) than expected by chance. Moreover, for each target area in the AC and rsFC fingerprints, paired *t*-tests were used to test the significance of the connectional differences between the results for each pair of subregions.

## RESULTS

### CBP of the NAc

Because it presented significantly higher registration accuracy, NABC was chosen as the optimal registration method for the local brain images that were limited to the NAc. Forty subjects were selected for the PDT-CBP and the rsFC-CBP. All three schemes consistently constrained the maximum clustering number to 4. The resulting parcels were visualized in multislices (Fig. 2).

The 2-cluster solution in three schemes as well as the 3-cluster solution in the PDT-CBP, presented highly symmetric topological distributions across the hemispheres. Additionally, we observed good convergence between the three schemes in the 2-cluster solution. Shifting attention to the data metrics, compared to the 3- and 4-cluster

solutions, the 2-cluster solution was clearly superior for all the data metrics. Specifically, the optimal solution according to the Dice coefficients was, in order,  $2 > 3 > 4$ , while according to the VI, the order was  $2 > 4 > 3$  (Fig. 3; see Supporting Information Results II.1). In addition, the topological distribution of the 2-cluster solution corresponded well to the well-accepted shell-core dichotomy. Taking all of these points together, we chose the 2-cluster solution as the optimal solution in this study. We named the ventral-caudal portion the “shell-like subdivision” and the dorsal-rostral portion the “core-like subdivision” based on the anatomical shell-core organization. Subsequently, consensus clusters were generated as the final multimodal parcels, which were composed of seed voxels that were consistently assigned across the three schemes. The shell-like subdivision (left: 350 mm<sup>2</sup>; center-of-gravity (COG) in mm coordinates: [−8.87 8.45 −9.29]; right: 321 mm<sup>2</sup>; COG: [8.93 8.61 −8.80]) and the core-like subdivision (left: 327 mm<sup>2</sup>; COG: [−10.72 16.19 −5.62]; right: 314 mm<sup>2</sup>; COG: [10.67 16.90 −5.49]) in standard MNI space were visualized in multislices and in 3D (Fig. 3).

### Anatomical Connectivity of the NAc Subregions

For visualization purposes, the AC patterns of the NAc subregions were thresholded at 70% and portrayed using MRICron (Fig. 4A). 18 target areas that met the criteria were extracted to build the AC fingerprints (Fig. 5A; Supporting Information Table S4).

### Cortical Areas

The connections with the two subregions were primarily concentrated in the ventral prefrontal region [Heidbreder and Groenewegen, 2003] and ACC, and relatively weakly with areas that included the temporal pole (TP), anterior parahippocampal gyrus (paraHIPPA), and anterior temporal fusiform cortex (TF.a). Two NAc subregions connected with the ventral prefrontal lobe via the forceps minor or, more specifically, the accumbofrontal fasciculus [Rigoard et al., 2011], but with obviously different connectional junctions and strengths. The shell-like subdivision connected with the mediocaudal regions, that is, the medial prefrontal cortex (MPFC; BA14), medial orbitofrontal cortex (OFC.m; medial part of BA13), and subcallosal cortex (SCC; BA25), while the core-like subdivision connected with the rostralateral prefrontal cortex, that is, the medial frontal pole (FP.m) and BA47. The shell-like subdivision also showed a significantly stronger connection with the ACC. In addition, the three weak connection areas aforementioned showed prominent connections with the shell-like area via the uncinate fasciculus.

In short, as shown by the quantified connectional fingerprints, the shell-like subdivision presented significantly stronger connections than the core-like subdivision with all the cortical areas in its connectional family, with the exception of the FP (see Supporting Information Results



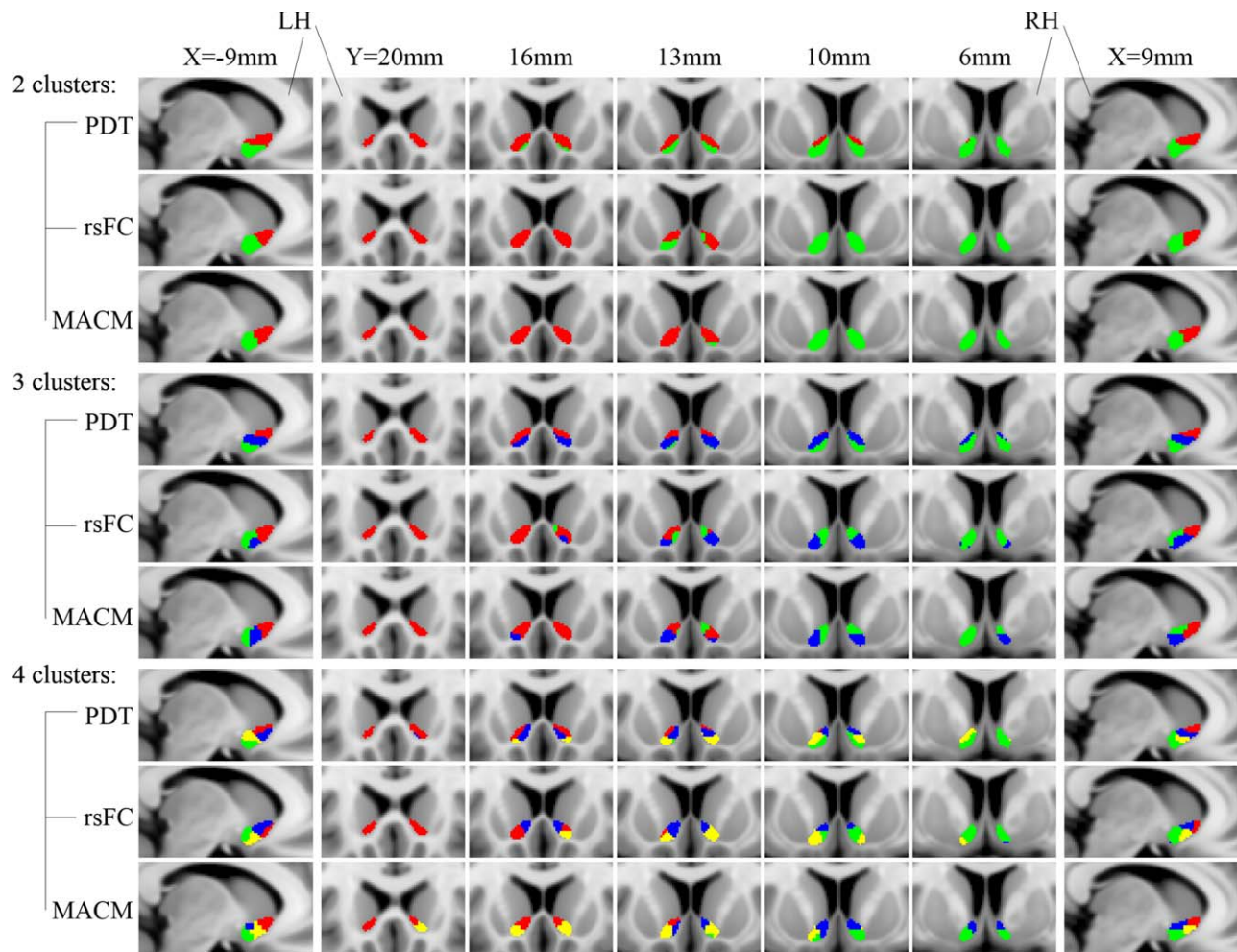


**Figure 2.**

Connectivity-based parcellation of the human NAc. For comparison and visualization purposes, the maximum probabilistic maps (thresholded at  $>50\%$ ) of the NAc subregions for  $k = 2, 3,$  and  $4$  using PDT, rsFC, and META are shown in a multislice presentation. LH: left hemisphere; RH: right hemisphere.

II.3). All the aforementioned connections, except those to the ACC, and OFC, were consistent with earlier reports [Haber et al., 1995; Parkinson et al., 2000; for reviews, see Basar et al., 2010; Salgado and Kaplitt, 2015]. The disagreement in the OFC was resolved by using the finer-grained frontal atlas described below. A possible explanation for the areas with weak connections is presented in the Supporting Information Results II.3.

### Subcortical Structures

All the limbic structures in the combined atlas, except the Pa, showed extensive connections with the two NAc subregions. For example, the HIPPO was connected via the fimbria-fornix fiber bundle [DeFrance et al., 1985] and the CPU via intra-striatal projections [van Dongen et al., 2005].

For these, the shell-like area showed a significantly stronger connection with the HIPPO and the AMYG but a significant weaker connection with the Pa and the Ca; no significant differences were found with the Pu. Some other important connections included connections with the midbrain (MidB) and the thalamus (THA) subregions, two strong connection areas (THA.preF and THA.T), and two weak connection areas (THA.O and THA.postP); all of these showed significant connections with the core-like subregion.

In short, the shell-like subdivision had prominent connections with the HIPPO and AMYG, while the core-like subdivision had prominent connections with the Ca, Pa, MidB, THA.preF, THA.T, and THA.postP. No significant differences were found in the Pu or the THA.O.

After further permutation tests comparing the fingerprints of the two subregions, the observed was greater



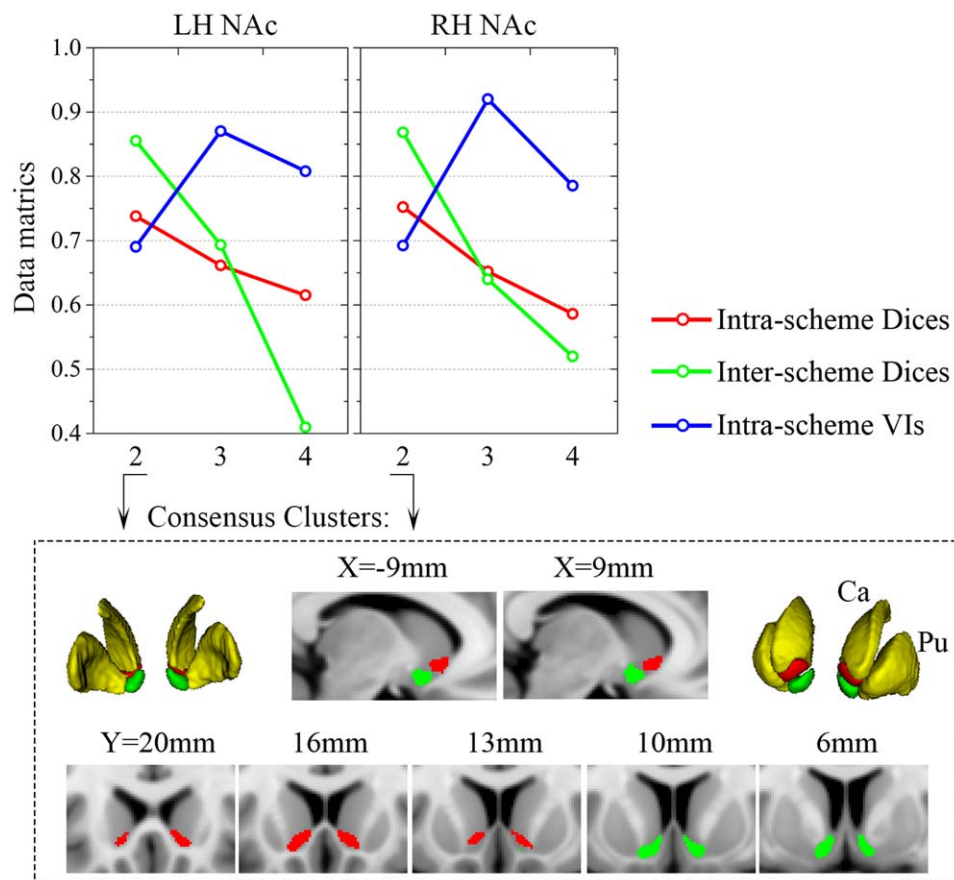


**Figure 3.**

Clustering metrics and the consensus clusters. Top panel: the mean Dices for the parcels of the three schemes (across subjects for PDT- and rsFC-CBP; across filter-sizes for MACM-CBP) were averaged as the intra-scheme Dices (red lines). The final parcels of the three schemes were used to calculate the inter-

scheme Dices (green lines) and the intra-schemes VIs (blue lines) (detailed in Supporting Information Methods I.5). Consensus clusters of the 2-cluster solution are shown as multislices and in 3D in the low panel. Ca: caudate; Pu: Putamen.

than the criterion in the right tail, so we rejected the null hypothesis as not being a likely explanation for such an observed difference, that is, the two fingerprints were “far” from each other in that the shell-like and core-like subdivisions had clearly distinct AC profiles. In the same way, we observed “close” fingerprints across the corresponding subregions between hemispheres (Supporting Information Fig. S7), reflecting the inter-hemispheric symmetry of the AC pattern.

### Resting-state Functional Connectivity of the NAc Subregions

We examined the voxel-wise whole-brain common and specific rsFC patterns for the NAc subregions (Fig. 4B and Supporting Information Fig. S5, for the peak coordinates see Supporting Information Table S1). 20 target areas were

extracted to build the rsFC fingerprints (Fig. 5A; Supporting Information Table S4).

The cortical areas that held positive rsFC in common with the two NAc subregions were concentrated in the SCC, insular (INS), FP, ACC (prelimbic and dorsal portions), and the paracingulate cortex (paraCC). The subcortical structures that connected to both subregions included the CPu, Pa, THA, and MidB. In addition, both left NAc subregions had activations with the OFC (BA11); both right NAc subregions had activations with the HIPP and paraHIPP.a.

The brain areas that had negative rsFC with both NAc subregions were concentrated in the superior parietal (SPL), inferior parietal lobules (IPL), precuneus, and some extensional areas. Additionally, a greater number of negatively connected areas, including the temporal (middle/inferior temporal gyrus) and frontal (middle/inferior frontal gyrus) lobe areas and the precentral gyrus, were found in the right than in the left hemisphere.

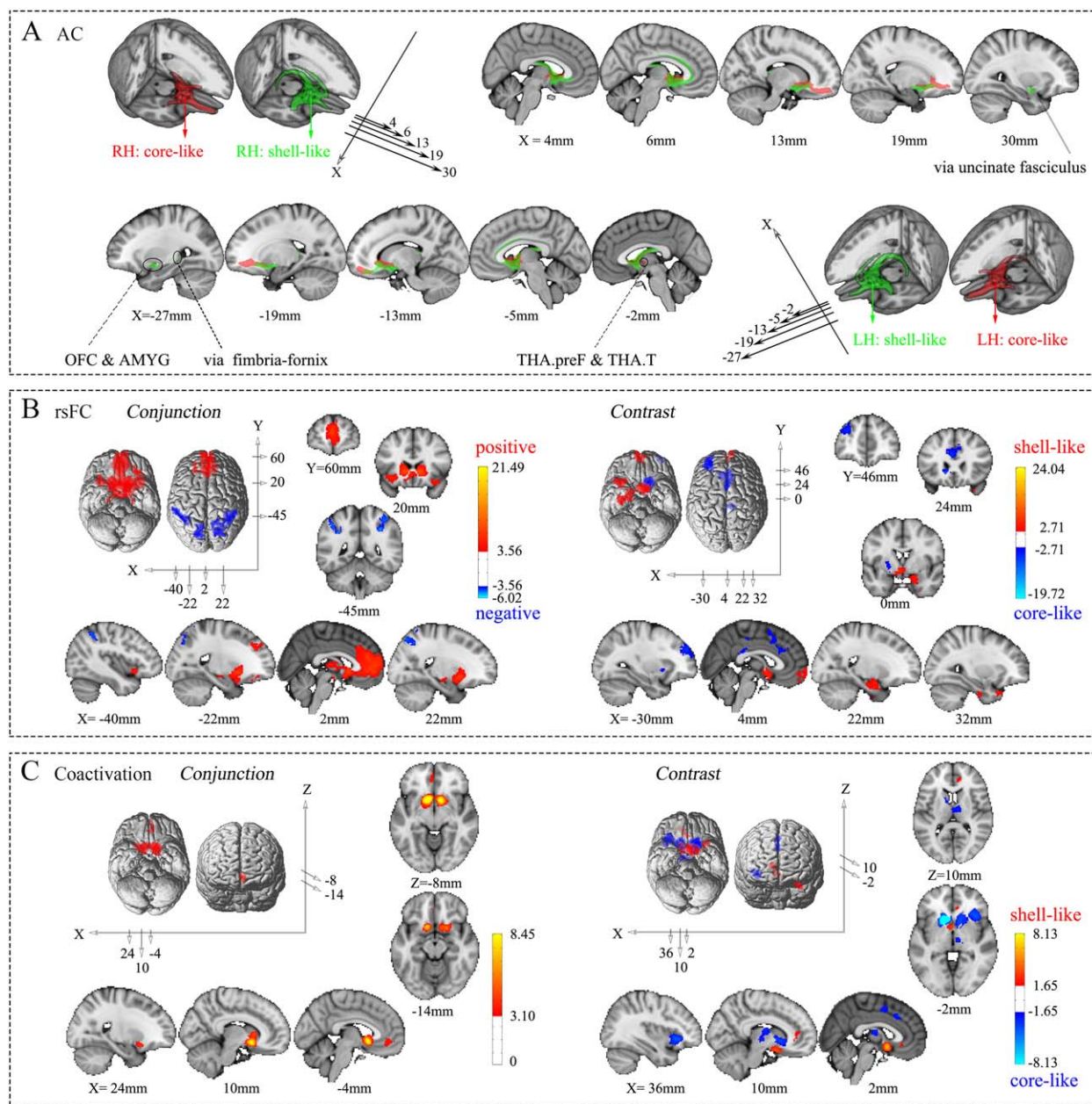


**Figure 4.**

Connectivity patterns of the shell-like and core-like subdivisions. (A) Population maps of the probabilistic tractography results from the two NAc subregions in the bilateral hemispheres were thresholded at 70% and are portrayed on the MNI152 standard brain in 3D and multislice presentations, respectively. (B) Conjunction and contrast analyses of the voxel-wise rsFC of the two NAc subregions in the left hemisphere. The former shows the

common positive and negative connections, using red–yellow and blue–cyan color ranges, respectively, while the latter shows the specific connections with the shell-like and core-like subdivisions, using red–yellow and blue–cyan color ranges, respectively. (C) Conjunction and contrast analyses of the voxel-wise coactivation of the two NAc subregions in the left hemisphere. For specifics about the color ranges, please refer to the explanation in (B).

Specific differences in the rsFC patterns between the two subregions were examined by paired *t*-tests. The shell-like subdivision had significant rsFC with the SCC

and AMYG. In addition, the left shell-like subdivision had prominent connections with many other areas, including the HIPp, paraHIPp, FP.m (BA10/11), TF.p (BA20), and

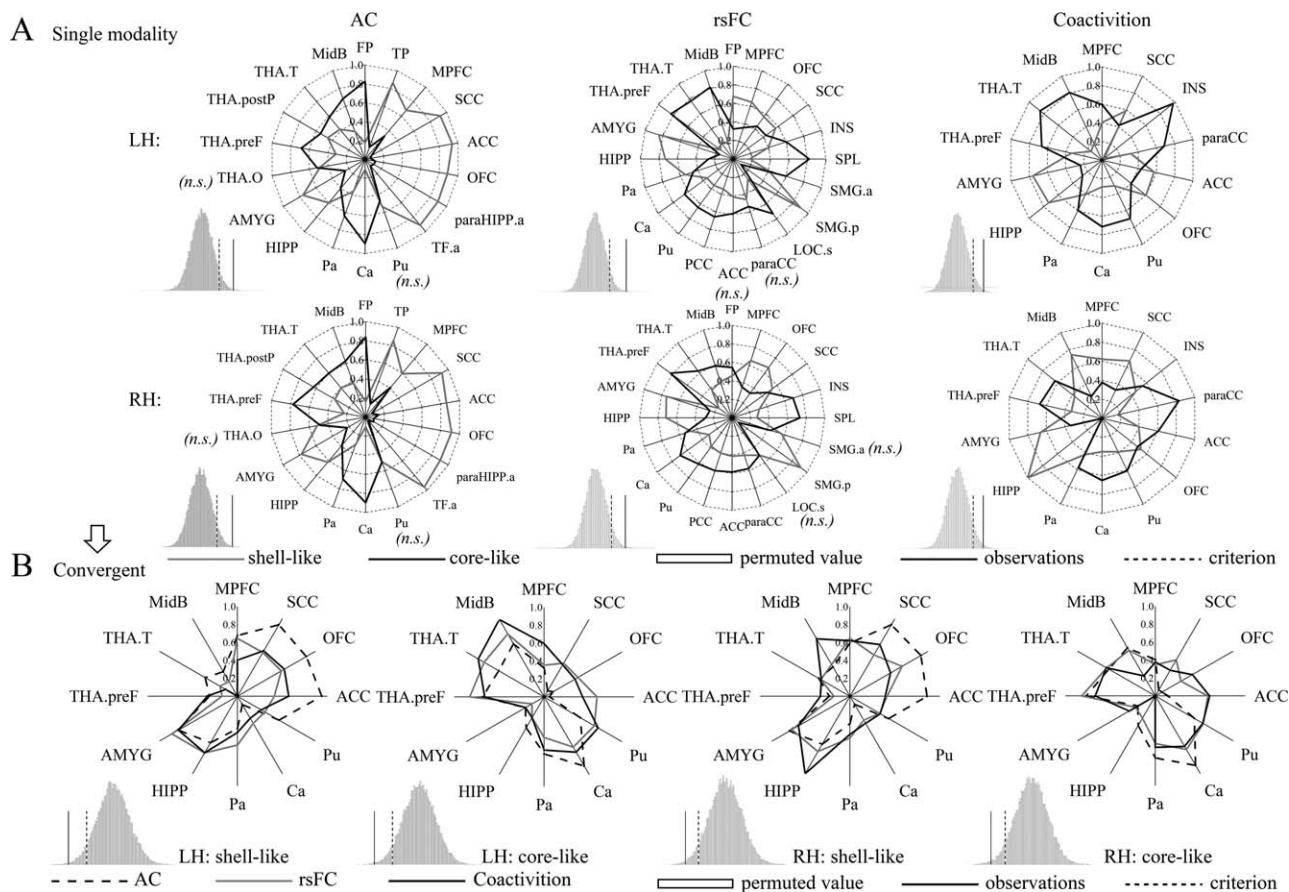


**Figure 5.**

Connectivity fingerprints of the shell-like and core-like subdivisions. (A) Left, middle, and right two panels show the AC, rsFC, and coactivation fingerprints, respectively. For each target area, the connective differences between the two subregions with this target area were tested using a paired samples *t*-test (HCP-40 dataset). “n.s.” indicates that no significant difference was found. For the fingerprint, the differences between the two NAc subregions was greater than expected by chance after the permutation tests (histograms); that is, the observation was greater than the criterion, indicating clearly distinct profiles for the shell-like

and core-like subdivisions in the three connection types. (B) The intersection of the fingerprints across three connection types was extracted as the convergent connective family. The new AC, rsFC, and coactivation fingerprints of the bilateral NAc subregions are shown in blue, red, and cyan lines, respectively. Permutation tests showed that the difference between these fingerprints was smaller than expected by chance, indicating convergent connective profiles across three modalities for the shell-like and core-like subdivisions.

TP, while the right shell-like subregion had a prominent connection with the MPFC. In contrast, the core-like subdivision had significant rsFC with the Ca, Pu, ACC, and FP.I (BA46). Additionally, the left core-like subregion also had a prominent connection with the posterior cingulate cortex (PCC), and the right core-like subdivision had a prominent connection with the INS.

The results from the fingerprint analyses were similar to the above results from the voxel-wise connectivity (detailed in Supporting Information Results II.4); in brief, the shell-like subdivision had significant cortical connections with the MPFC, OFC, SCC, and supramarginal gyrus posterior division (SMG.p; weak connection) and significant subcortical

connections with the HIPP and AMYG. In contrast, the core-like subdivision had significant cortical connections with the INS, SPL, ACC, paraCC, and PCC (weak connection) and significant subcortical connections with the CPu, THA.preF, THA.T, and MidB. Some other target areas, including the FP, SGM.a, lateral occipital cortex superior division (LOC.s), and Pa, were inconsistent across the hemispheres; a possible explanation is provided in the Supporting Information Results II.4.

After further permutation tests of these fingerprints across the subregions and hemispheres (Supporting Information Fig. S7), we got results similar to those from the AC fingerprints, in that the shell-like and core-like



subdivisions had clearly distinct rsFC profiles but symmetric connectivity patterns between the hemispheres.

### Task-Dependent Coactivation of the NAc Subregions

We further examined the coactivation patterns of the subregions and their conjunctions and contrasts analyses (Fig. 4C and Supporting Information Fig. S6, the peak coordinates were reported in Supporting Information Table S2). 14 target areas were extracted to build the coactivation fingerprints (Fig. 5A; Supporting Information Table S4; see Supporting Information Results II.5).

In brief, common coactivation areas with both NAc subregions included the SCC, Ca, and Pu. In addition, the left NAc subregions had a common coactivation with the paraCC (prelimbic portion), while the right NAc subregions had common activations with the THA and AMYG (anterior and central portions).

The brain areas that had specific coactivations with the shell-like subdivision were primarily concentrated in the SCC, HIPPI, and paraHIPPI. In addition, the left shell-like subdivision had a prominent coactivation with the OFC; the right shell-like subdivision had a prominent coactivation with the AMYG (basal portion). In contrast, the core-like subdivision had prominent coactivations with the CPu, INS, THA, and dorsal ACC/paraCC. The left core-like subregion also had a prominent coactivation with the MidB.

Unlike the findings from the AC and rsFC fingerprints, the fingerprints were asymmetric between the hemispheres. A possible explanation for this asymmetry is detailed in the Supporting Information Results II.5. Importantly, the coactivation profiles of the two NAc subregions still showed significant differences after the permutation tests.

### Conjunction Between the rsFC and MACM

Like the results reported by Hardwick et al. [2015], in this study, most areas found to be activated according to the MACM were also activated in the rsFC study. We reported the peak coordinates of the areas identified in both the rsFC and MACM analyses in Supporting Information Table S3.

The brain areas identified by both the rsFC and MACM analyses as connected with the shell-like subdivision were fairly localized bilateral clusters in the SCC, CPu, and the prelimbic ACC. Both types of analyses also showed connections between the left shell-like subdivision and the AMYG and paraHIPPI.a and between the right shell-like subdivision and the parietal lobes, THA, MidB, and INS. In comparison, both methods identified a concentration of connections between the core-like subdivision and the SCC, CPu, THA, INS, FP, ACC, and paraCC (prelimbic and dorsal portions) as well as between the right core-like subdivision and the parietal lobes.

### Convergent Connection Patterns Across Modalities in Fingerprints

The fingerprints of the three modalities were overlaid and their intersections, 12 target areas, were extracted to build convergent connection patterns for an across-modalities comparison. (Fig. 5B; Supporting Information Table S5). Interestingly, these surviving target areas included the same major areas that previous research suggested as being connected with the NAc [for reviews see Floresco, 2015; Salgado and Kaplitt, 2015]. These areas included the primary cortex afferent from the MPFC; SCC; ACC; subcortical structures, including the HIPPI and AMYG; the adjacent areas of the CPu; and important projections from the MidB and thalamic subregions.

Differences in the connectivity pattern across the modalities was localized to target areas, such as the TP and INS, that emerged in one modality but not the others and to target areas whose connective tendency to NAc subregions such as the FMed and ACC, was inconsistent. The same conflicting connections were also reported by Baliki et al. [2013]. Nevertheless, most of the areas that had emerged from these modalities were retained in the convergent fingerprint, and only the weak connective areas were eliminated. Additionally, when using the unified connective family, the permutation tests confirmed “close” relationships between the fingerprints from each of the three modalities (Fig. 5B and Supporting Information Fig. S7). All these together reflected convergence between the three modalities.

### Finer Frontal Cortical Connectivity Profiles

Since our finding that the OFC had prominent connections with the shell-like subdivision in the fingerprint was inconsistent with earlier studies [Basar et al., 2010; Salgado and Kaplitt, 2015], we resolved this difference by using a finer frontal atlas. The name and the corresponding locations of some of the regions in this atlas are portrayed in Figure 6. The AC fingerprints were approximately symmetric between the hemispheres, clearly showing that the shell-like subdivision had a prominent connection with mediocaudal regions such as 14m, 13, and 25 and the core-like subdivision had a prominent connection with areas of the rostralateral prefrontal cortex, such as 11m, 11, 47o, and 47m. Interestingly, such territoriality, with the areas clearly segregated according to their differential connections with the shell-like and core-like subdivisions, is quite consistent with a previous meta-analysis about reward and punishment [Kringelbach and Rolls, 2004].

## DISCUSSION

Three parcellation schemes, PDT-CBP, rsFC-CBP, and MACM-CBP, from complementary neuroimaging modalities, that is, dMRI, rs-fMRI, and task-dependent coactivity,



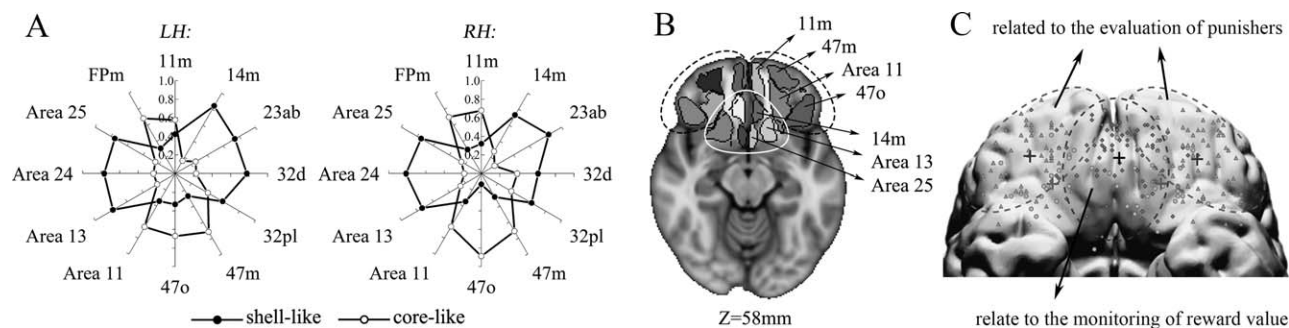


**Figure 6.**

Specific frontal cortical connectivity profiles. (A) AC fingerprints for the NAc subregions with target areas that met the criteria, these target areas were extracted from a finer-gained frontal atlas. (B) Axial slices ( $Z = 58$  mm) through the MNII52 standard brain with the AC areas overlaid regions that had a prominent connection with the shell-like subdivision are wrapped in a white circle, while regions wrapped in black dotted circles are

respectively, were used to parcellate the human NAc. The 2-cluster result was chosen as the optimal solution because of its clear superiority in data metrics and in its relationship to the well-known morphologic subdivision. Consensus clusters across the three schemes were subsequently yielded as the final parcels. We characterized three types of connectivity patterns of the parcels from voxel-wise and fingerprint perspectives and compared the connectivity patterns across hemispheres, modalities, and subregions. The results showed inter-hemispheric symmetry, a high level of convergence, clear divergence across the modalities, and, most importantly, significant heterogeneity between the subregions. The result also confirmed the primary connections of the shell and core from earlier animal reports, supporting dissociable roles of the shell and core, to some degree. Furthermore, the resulting data-driven NAc parcels may aid further research into the NAc subregions, particularly in neuroimaging.

### Considerations of the Methodological Basis

Local microstructural/molecular features and the holistic connective architecture are indicated to be complementary and correlative, which are both implicated in determining a region's function [cf. Barbas and Rempel-Clover, 1997; Fan et al., 2016; van den Heuvel et al., 2015]. However, the gross correspondence of the parcellation results based on different features or even sub-features, for example, different immunohistochemical markers or different connection types in this study, still remains unclear, weaker- or even noncorresponding results exist in many studies [Fan et al., 2014; Liu et al., 2013; Moerel et al., 2014; Wang et al., 2016]. For example, both left and right inferior parietal lobule (LIPL/RIPL) were parcellated into seven regional cytoarchitectonic subregions [Caspers et al.,

2006], but three receptor distributed subregions [Caspers et al., 2013] and five tractographically defined subregions [Mars et al., 2012; Wang et al., 2012]. Thus, more work is needed to untangle the complex relationship between these features.

In this study, the new evidence of the NAc's parcellation results was provided based on three types' connections. An alternative hypothesis was that these parcels based on different types' long-range connections could better correspond with each other and with microstructural subregions, and the key connections could be in line with trace neural connections, that is, the correlations exist among macro-connections or/and microstructures in human NAc. And, if the hypothesis is confirmed, the availability of our results is confirmed in some degree as well.

### Connectivity-Based Parcellation

How to be sure that the optimal solution to a parcellation scheme has been identified remains an open question [Thirion et al., 2014], but it is clear that fine connective distinctions can be detected as imaging solutions or methods improve and that finer grained parcellations will follow. Existing anatomical and histochemical studies have most frequently subdivided the NAc into 2, 3, or 4 clusters. An exception was a "patch-matrix" organization [Humphries and Prescott, 2010], which subdivided the NAc into more subregions, but this was difficult to investigate in this study because of limitations in both data quality and the distance constraint algorithm used in our parcellation. For these reasons, we set the maximum value of the clustering algorithm to 4. For similar reasons, Baliki et al. [2013] used PDT-CBP to directly subdivide the human right NAc into a pshell and a pcore to match the well-accepted shell-core dichotomy.

As previously mentioned, the 2-cluster solution was chosen as the optimal solution because of its clear superiority in the data metrics compared to the other two solutions as well as because of its correspondence with the well-accepted dichotomy. Specifically, both the Dice and the VI indicated that the 3-cluster solution was not the optimal one, and the 4-cluster solution barely met the secondary criteria of the mean VIs but had a poor Dice. Therefore, both solutions were rejected, although they could be considered for further study using a better scheme or/and more accurate data. The parcels in selected 2-cluster solution confirmed the hypothesis mentioned above that the better correspondence among parcels based on different features/sub-features exists in human NAc. And this further enabled us to obtain consensus clusters, like the procedure used in previous studies, such as Bzdok et al. [2013] who got consensus clusters for the right temporo-parietal junction using rsFC-CBP and MACM-CBP and Wang et al. [2015] who obtained consensus clusters for the superior parietal lobe using the same three schemes as we used. We chose these multimodal consensus clusters as the final parcellation for the subsequent connectivity analysis. The comparisons between our result and early results were detailed in Supporting Information Results II.2.

### Connectivity Patterns of the NAc Subregions Support Their Putative Functions

As reviewed in Floresco [2015] and Humphries and Prescott [2010], the NAc appears to integrate cognitive, mnemonic, and emotional signals primary from the frontal lobe, HIPp, and AMYG, respectively, and turn them into action via output to the ventral pallidum (VP) and other subcortical motor effector sites. Thus, the NAc may help to determine the direction and intensity of behavior. Earlier studies found functional and anatomical heterogeneity in the NAc. Therefore, we used neuroimaging to investigate these subregions' unique connections to try to understand how their specific functions are indicated by their unique connections [Johansen-Berg et al., 2004; Sporns et al., 2005].

In summary, although between-hemispheric differences were found in some areas using a voxel-wise approach, the connectivity fingerprint, obtained by finding the mean connectivity strength of the target areas obtained from the combined atlas, showed good between-hemispheric symmetry except for between-hemispheric differences in coactivity. Additionally, most areas that had weak connective strength in any of the three types of fingerprints, such as the FP and PCC, which were weak in coactivity, and the SPL and SMG, which were weak in both AC and coactivity, were excluded from the convergent connection family. This further enhanced the reliability of the comparison of the fingerprints because, logically, weak connections may be more susceptible to errors. Permutation tests on these unified convergent connections confirmed convergence across the three

modalities by revealing "close" relationships between the fingerprints. Thus, the connections we discuss below can be understood as referring to any of the three modalities, unless there was some reason for special emphasis with respect to one of the modalities. Later in this discussion, the significant heterogeneous connection patterns across the NAc subregions that underlie their specific functions will be discussed in connection with each specific subregion.

### Consensus Target Areas

As shown above, we obtained 12 consensus target areas that possessed all three types of connections with the two NAc subregions and used them for the convergent connection fingerprints. Having only a few (i.e., 12) consensus target areas in the fingerprints avoided the risk of overfitting the fingerprint [Mars et al., 2016]. Compared with the 10 prespecified target areas in Baliki et al. [2013], two areas, the INS and paraCC, were excluded from our convergent connection family because of their weak direct- (AC) but rich indirect-connection (rsFC or coactivity) with the NAc. Earlier studies reported that projections from the agranular INS to the core, including direct- [Brog et al., 1993] and indirect- [Wright and Groenewegen, 1996] projections via the thalamic nucleus as well as projections from the dorsal and ventral agranular insula region only reach the lateral core and lateral shell, respectively [Humphries and Prescott, 2010]. In addition, the paraCC exhibits significant morphological variations in the paraCC sulcus across subjects, sexes, and hemispheres [Fornito et al., 2006; Leonard et al., 2009], presenting an absence of the rich limbic connections characteristic of the ACC in non-human primates [Paus, 2001].

In addition, the CC was replaced by the ACC, which has been reported to project to the restricted portion of the rostromedial NAc. Additionally, the MPFC has been found to have extensive and distinct projections to the shell and core [Heidbreder and Groenewegen, 2003; Zahm, 1999]. The basal ganglia, which include all the subcortical nuclei, had distinct connections with the two subregions but were replaced in our work by their sub-structures, that is, the Pu, Ca, and Pa. In addition, DA-synthesizing neurons in the MidB play an important role in regulating most of the functions of the NAc [Ikemoto, 2007; Volkow and Morales, 2015]. Some nuclei of the thalamus, which reportedly project to the shell and core [Berendse and Groenewegen, 1990], have an important role in regulation, such as in aversive memory [Zhu et al., 2016]. Based primarily on these important connection areas that were found in the convergent fingerprints, we will briefly discuss the possible functions of our final NAc subregions.

### Shell-like Subdivision

Located in the ventromedial NAc, the shell-like subdivision corresponds to the anatomical shell subregion. The

major function of the shell was summarized as “stay on task” by Floresco [2015]. This expression shows the association of this area with reward-related goals that have already been obtained or are going to be obtained in complex environments by suppressing irrelevant, less- or non-rewarding stimuli. This possible function was primarily raised by numerous lesion or inactivity experiments in animal models but was supported by the connectivity patterns of the shell-like subdivision in this neuroimaging study.

### **Cortical Areas**

The shell-like subdivision had prominent cortical connections, including those with the MPFC, OFC, and SCC. Using a finer-grained frontal atlas, we found that this connection is prominently concentrated in the medio-caudal prefrontal cortex. This is consistent with findings from previous research, for example, that the connections with BA 25 are notably restricted to the medial shell [Heidbreder and Groenewegen, 2003]. The specific connection profile from neuroimaging also agreed with a medial-lateral distinction of the ventral prefrontal cortex based on a unitary appetitive response to rewards or punishments, according to a meta-analysis by Kringelbach and Rolls [2004], and further supported a prominent reward role for the shell-like subregion. However, the ACC, as aforementioned, showed an unexpected result in AC and coactivation (with the left shell-like subdivision), which might, as with the result for the CC in Baliki et al. [2013], have been caused by different types of connections. Functionally, the medio-caudal prefrontal cortex, especially area 25, which has projections to the NAc, appears to play a central role in suppressing strategies [Peters et al., 2008].

### **HIPP and AMYG**

The shell-like subdivision had prominent limbic connections with the HIPP and AMYG, findings which were consistent with former research findings about the shell. HIPP formation projections from the subiculum and CA1 regions were notably restricted to the shell via the fimbria-fornix fiber bundle [Groenewegen et al., 1987]. This was confirmed by the AC, which functionally appears to be involved in the spatial navigation of different environmental stimuli and the recognition of novelty [Ito et al., 2008; Mannella et al., 2013]. The basolateral AMYG primarily projects to the shell [Wright and Groenewegen, 1996] and appears to be involved in the complicated function of encoding the value of stimuli and predicting their appetitive or aversive consequences to adjust the motivational level [Cardinal et al., 2003].

### **MidB**

The cortical and limbic inputs impinge on and may integrate into the NAc [French and Totterdell, 2003] for the

regulation of DA from the MidB [Lodge and Grace, 2006]. DA has been reported to play different roles in the NAc shell and core, involving complementary or even antagonistic functions in some circumstances [Baudonnat et al., 2013]. On the basis of its primary origin from the VTA, the shell was hypothesized to be functionally associated with the mesolimbic dopamine system and to play a critical role in biasing decision-making when a reward is uncertain [Dreyer, 2010; Stopper and Floresco, 2011]. But in this study, the MidB was involved, rather than the subregions of the VTA, so we only observed a weaker connection with the shell-like area, compared to the core-like subdivision. Finer-grained connection patterns may be detectable in the future.

### **Other Subcortical Structures**

It is clear from their anatomy and histochemistry that the dorsolateral and the ventromedial ventral pallidum (VP) are the major output locations for the shell and core, respectively [for reviews, see Basar et al., 2010; Salgado and Kaplitt, 2015]. In this study, limited by the lack of a VP-atlas for human neuroimaging, we only observed the Pa had a weak connection with the shell-like area. Some other structures, the CPu and THA, which both had weak connections with the shell-like area, will be discussed below in connection with the core-like subdivision. In addition, prominent connection between the two subregions were found in the voxel-wise connection patterns, a finding which was consistent with former research indicating that the shell receives extensive projections from the core [van Dongen et al., 2005]. Functionally, this connection may involve the passing of the expected value of each associative cue and behavior in response to salient stimuli [Day et al., 2011]; according to probabilistic reinforcement learning theory, the resulting predicted error could then be brought back to prefrontal cortex through the cortico-striato-thalamo-cortical loop to update subsequent similar action-outputs [for review, see Dolan and Dayan, 2013].

In short, our neuroimaging research revealed prominent connections of the shell-like subdivision with the medio-caudal part of the prefrontal cortex, HIPP, and AMYG. This evidence indicated that the function of the shell-like subdivision is to maintain the association with the best available reward by suppressing the less- or non-rewards stimuli. The connection with medio-caudal prefrontal cortex also supports this prominent reward role for the shell-like area.

### **Core-like Subdivision**

The core-like subdivision, located in the dorsolateral NAc, corresponded to the anatomical core subregion. Functionally, the core has been deemed to have the same goal as the shell but with a distinctive way of selectively implementing the specific goal-directed actions to approach a new reward-related goal in complex environments. This has

been summarized as “Go to it” by Floresco [2015]. This specific implementation also received neuroimaging support from our findings about the connectivity patterns of the core-like subregion.

### **Cortical Areas**

High frequency DBS animal experiments suggested cortical connections between the core and the olfactory cortex [McCracken and Grace, 2007]. This is consistent with the core-like area’s connectivity profiles gained by using a more finely divided frontal atlas. The same regions of the lateral OFC have also been reported to be involved with encoding punishments [Kringelbach and Rolls, 2004]. These findings supported the prominent aversive role of the core-like subdivision, that is, that it has an antagonistic interaction with the shell-like area. Another major cortical connection area was with the ACC, part of the branch of the cortico-striato-thalamo-cortical loop, which showed a prominent connection with the core, as was confirmed by the connection patterns (except for those obtained using AC) of the core-like subdivision. Functionally, the prelimbic ACC had been reported to be involved in working memory for action-outcome-based sequencing [Coutureau and Killcross, 2003] by being updated constantly through the aforementioned loop. Thus it may provide action information to the core-like subdivision to enable a shift toward a new action when more rewarding stimuli occur.

### **AMGY and THA**

The weak connection between the core-like area and the AMYG may be involved in the regulation of Pavlovian and instrumental conditioning [Cardinal and Everitt, 2004; Everitt et al., 2001]. This connection, along with the cortical connection, may function to predict cues and salient stimuli [Day et al., 2010; Roesch et al., 2007] by encoding the subjective value of the stimuli and selecting the action that tends toward the best available option [Mogenson et al., 1980]. The THA’s prominent connection with the core-like subdivision was primarily concentrated in the THA.preF and THA.T, that is, the prefrontal- and temporal-specific thalamus subregions, areas that have also been reported to be required for the expression of aversive withdrawal symptoms [Zhu et al., 2016], another indication of the specific-aversive role of the core-like subdivision.

### **MidB**

Another MidB subregion, the SN [Bjorklund and Dunnett, 2007] was found to have a prominent connection with the core. The finding that DA primarily originates from the SNc may indicate that, functionally, the core, like the dorsal striatum, is associated with the nigrostriatal dopamine system [Deutch, 1992] and plays a role in motor control [Bassareo et al., 2007]. DA originating from the VTA, however, may be involved in selectively facilitating

a flexible response to reward-related stimuli [Saunders and Robinson, 2012]. In this study, as stated above, we observed a strong connection with the MidB rather than with its subregions. Therefore, the connection with the MidB subregion needs further study.

### **Other Subcortical Structures**

The core-like subdivision showed prominent connections with the CPu and Pa. Two perspectives may shed light on these connections. First, there may not be a sharp border between the NAc and the CPu, so the input and output projections of the NAc neurons blended into neighboring regions [Maurice et al., 1999]. The second possible explanation is that the two neighboring regions have extensive interconnections via intra-striatal projections [van Dongen et al., 2005]. In this case, a strong connection with the core-like area could have resulted from the larger contact area.

In short, our neuroimaging research revealed prominent connections of the core-like subdivision with the lateral OFC and ACC as well as with the CPu, MidB, THA.preF, and THA.T subcortical structures. These connections may provide evidence that the core-like subdivision plays a greater role in selectively instigating an approach toward stimuli associated with new best available rewards or with safety, that is, task switching from the current stimulus to a more rewarding one after a Pavlovian subjective prediction about stimuli or cues in a complex environment. In addition, the neurocircuits of this subregion further supported its prominent aversive role.

In general, the differences in the connection patterns provided by the three types of connections roughly supported the concept that the two NAc subregions have different, or even antagonistic, functions [Baudonnat et al., 2013]. However, these functions of the two subregions must be interrelated and complementary with each other, as indicated by their anatomical and functional interconnections, including direct and indirect connections via multiple circuits. A comprehensive understanding of the characteristics of the NAc subregions may eventually be realized by studying their anatomical and functional (task-independent and task-dependent) connection patterns using many related biological experiments.

## **LIMITATIONS AND IMPROVEMENTS**

Many factors, such as data quality and the registration method, may impair the accuracy of parcellations and the characterization of the connectivity patterns (see Supporting Information Limitations and Improvements). In this study, we selected subjects from high-quality HCP data, used the NABC registration method to relieve these impacts, and got well-overlapped consensus clusters from the three modalities. But many issues raised by this study, such as obtaining finer NAc parcellations and re-



testing of the inconsistent connections across modalities, still require further research using better parcellation schemes, higher-quality data, or a finer brain atlas in the future.

## CONCLUSIONS

We parcellated the human NAc using three data-driven parcellation schemes based on high-quality neuroimaging data along with some improvements. The 2-cluster solution was chosen as the optimal one. The consensus clusters in this solution across the three schemes were generated as the final parcels. Furthermore, the AC, rsFC, and coactivation patterns of these parcels were characterized from both voxel-wise and fingerprint perspectives. The latter was then used to compare the connectivity patterns across the hemispheres and subregions. The convergent connectional family was extracted and used for the comparisons across the modalities. We found symmetry between the hemispheres, convergence and divergence between the modalities, and clearly distinct patterns between the subregions. These convergent neuroimaging-derived connectivity patterns confirmed earlier findings from animal models and supported dissociable roles for the NAc subregions.

## ACKNOWLEDGMENTS

Data were provided by the Human Connectome Project, WU-Minn Consortium (Principal Investigators: David Van Essen and Kamil Ugurbil; 1U54MH091657) funded by the 16 NIH Institutes and Centers that support the NIH Blueprint for Neuroscience Research; and by the McDonnell Center for Systems Neuroscience at Washington University. The authors declare that the research was conducted in the absence of any commercial or financial relationships that could be construed as a potential conflict of interest. Extensive editing of both the content and the English was performed by Edmund F. and Rhoda E. Perozzi, PhDs.

## REFERENCES

- Aharon I, Beger L, Chabris CF, Borsook D (2006): Noxious heat induces fMRI activation in two anatomically distinct clusters within the nucleus accumbens. *Neurosci Lett* 392:159–164.
- Arts MP, Groenewegen HJ (1992): Relationships of the dendritic arborizations of ventral striatomesencephalic projection neurons with boundaries of striatal compartments. An in vitro intracellular labelling study in the rat. *Eur J Neurosci* 4: 574–588.
- Baldassano C, Beck DM, Fei-Fei L (2015): Parcellating connectivity in spatial maps. *PeerJ* 3:e784.
- Baliki MN, Mansour A, Baria AT, Huang L, Berger SE, Fields HL, Apkarian AV (2013): Parceling human accumbens into putative core and shell dissociates encoding of values for reward and pain. *J Neurosci* 33:16383–16393.
- Barbas H, Rempel-Clower N (1997): Cortical structure predicts the pattern of corticocortical connections. *Cereb Cortex* 7:635–646.
- Basar K, Sesia T, Groenewegen H, Steinbusch HWM, Visser-Vandewalle V, Temel Y (2010): Nucleus accumbens and impulsivity. *Prog Neurobiol* 92:533–557.
- Bassareo V, De Luca MA, Di Chiara G (2007): Differential impact of pavlovian drug conditioned stimuli on in vivo dopamine transmission in the rat accumbens shell and core and in the prefrontal cortex. *Psychopharmacology (Berl)* 191:689–703.
- Baudonnat M, Huber A, David V, Walton ME (2013): Heads for learning, tails for memory: Reward, reinforcement and a role of dopamine in determining behavioral relevance across multiple timescales. *Front Neurosci* 7:e175.
- Behrens TE, Johansen-Berg H, Woolrich MW, Smith SM, Wheeler-Kingshott CA, Boulby PA, Barker GJ, Sillery EL, Sheehan K, Ciccarelli O, Thompson AJ, Brady JM, Matthews PM (2003): Non-invasive mapping of connections between human thalamus and cortex using diffusion imaging. *Nat Neurosci* 6:750–757.
- Behrens TE, Berg HJ, Jbabdi S, Rushworth MF, Woolrich MW (2007): Probabilistic diffusion tractography with multiple fibre orientations: What can we gain? *Neuroimage* 34:144–155.
- Berendse HW, Groenewegen HJ (1990): Organization of the thalamostriatal projections in the rat, with special emphasis on the ventral striatum. *J Comp Neurol* 299:187–228.
- Bjorklund A, Dunnett SB (2007): Dopamine neuron systems in the brain: An update. *Trends Neurosci* 30:194–202.
- Blomstedt P, Sjöberg RL, Hansson M, Bodlund O, Hariz MI (2013): Deep brain stimulation in the treatment of obsessive-compulsive disorder. *World Neurosurg* 80:245–253.
- Brauer K, Hausser M, Hartig W, Arendt T (2000): The core-shell dichotomy of nucleus accumbens in the rhesus monkey as revealed by double-immunofluorescence and morphology of cholinergic interneurons. *Brain Res* 858:151–162.
- Breiter HC, Aharon I, Kahneman D, Dale A, Shizgal P (2001): Functional imaging of neural responses to expectancy and experience of monetary gains and losses. *Neuron* 30:619–639.
- Brog JS, Salyapongse A, Deutch AY, Zahm DS (1993): The patterns of afferent innervation of the core and shell in the “accumbens” part of the rat ventral striatum: Immunohistochemical detection of retrogradely transported fluoro-gold. *J Comp Neurol* 338:255–278.
- Bzdok D, Langner R, Schilbach L, Jakobs O, Roski C, Caspers S, Laird AR, Fox PT, Zilles K, Eickhoff SB (2013): Characterization of the temporo-parietal junction by combining data-driven parcellation, complementary connectivity analyses, and functional decoding. *Neuroimage* 81:381–392.
- Cardinal RN, Everitt BJ (2004): Neural and psychological mechanisms underlying appetitive learning: Links to drug addiction. *Curr Opin Neurobiol* 14:156–162.
- Cardinal RN, Parkinson JA, Marbini HD, Toner AJ, Bussey TJ, Robbins TW, Everitt BJ (2003): Role of the anterior cingulate cortex in the control over behavior by Pavlovian conditioned stimuli in rats. *Behav Neurosci* 117:566–587.
- Caspers S, Geyer S, Schleicher A, Mohlberg H, Amunts K, Zilles K (2006): The human inferior parietal cortex: Cytoarchitectonic parcellation and interindividual variability. *NeuroImage* 33: 430–448.
- Caspers S, Eickhoff SB, Geyer S, Scheperjans F, Mohlberg H, Zilles K, Amunts K (2008): The human inferior parietal lobe in stereotaxic space. *Brain Struct Funct* 212:481–495.
- Caspers S, Schleicher A, Bacha-Trams M, Palomero-Gallagher N, Amunts K, Zilles K (2013): Organization of the human inferior

- parietal lobule based on receptor architectonics. *Cereb Cortex* 23:615–628.
- Castro DC, Berridge KC (2014): Advances in the neurobiological bases for food ‘liking’ versus ‘wanting’. *Physiol Behav* 136:22–30.
- Castro DC, Terry RA, Berridge KC (2016): Orexin in rostral hot-spot of nucleus accumbens enhances sucrose ‘liking’ and intake but scopolamine in caudal shell shifts ‘liking’ toward ‘disgust’ and ‘fear’. *Neuropsychopharmacology* 41:2101–2111.
- Cauda F, Cavanna AE, D’Agata F, Sacco K, Duca S, Geminiani GC (2011): Functional connectivity and coactivation of the nucleus accumbens: A combined functional connectivity and structure-based meta-analysis. *J Cogn Neurosci* 23:2864–2877.
- Clos M, Amunts K, Laird AR, Fox PT, Eickhoff SB (2013): Tackling the multifunctional nature of Broca’s region meta-analytically: Co-activation-based parcellation of area 44. *Neuroimage* 83:174–188.
- Cohen AL, Fair DA, Dosenbach NU, Miezin FM, Dierker D, Van Essen DC, Schlaggar BL, Petersen SE (2008): Defining functional areas in individual human brains using resting functional connectivity MRI. *Neuroimage* 41:45–57.
- Coutureau E, Killcross S (2003): Inactivation of the infralimbic prefrontal cortex reinstates goal-directed responding in over-trained rats. *Behav Brain Res* 146:167–174.
- Day JJ, Jones JL, Wightman RM, Carelli RM (2010): Phasic nucleus accumbens dopamine release encodes effort- and delay-related costs. *Biol Psychiatry* 68:306–309.
- Day JJ, Jones JL, Carelli RM (2011): Nucleus accumbens neurons encode predicted and ongoing reward costs in rats. *Eur J Neurosci* 33:308–321.
- Deco G, Ponce-Alvarez A, Mantini D, Romani GL, Hagmann P, Corbetta M (2013): Resting-state functional connectivity emerges from structurally and dynamically shaped slow linear fluctuations. *J Neurosci* 33:11239–11252.
- DeFrance JF, Marchand JF, Sikes RW, Chronister RB, Hubbard JI (1985): Characterization of fimbria input to nucleus accumbens. *J Neurophysiol* 54:1553–1567.
- Desikan RS, Ségonne F, Fischl B, Quinn BT, Dickerson BC, Blacker D, Buckner RL, Dale AM, Maguire RP, Hyman BT, Albert MS, Killiany RJ (2006): An automated labeling system for subdividing the human cerebral cortex on MRI scans into gyral based regions of interest. *Neuroimage* 31:968–980.
- Deutch AY (1992): The regulation of subcortical dopamine systems by the prefrontal cortex: Interactions of central dopamine systems and the pathogenesis of schizophrenia. *J Neural Transm Suppl* 36:61–89.
- Dice LR (1945): Measures of the amount of ecologic association between species. *Ecology* 26:297–302.
- Dolan RJ, Dayan P (2013): Goals and Habits in the Brain. *Neuron* 2:312–325.
- Draganski B, Kherif F, Kloppel S, Cook PA, Alexander DC, Parker GJ, Deichmann R, Ashburner J, Frackowiak RS (2008): Evidence for segregated and integrative connectivity patterns in the human Basal Ganglia. *J Neurosci* 28:7143–7152.
- Dreyer JL (2010): New insights into the roles of microRNAs in drug addiction and neuroplasticity. *Genome Med* 2:92.
- Eickhoff SB, Laird AR, Grefkes C, Wang LE, Zilles K, Fox PT (2009): Coordinate-based activation likelihood estimation meta-analysis of neuroimaging data: A random-effects approach based on empirical estimates of spatial uncertainty. *Hum Brain Mapp* 30:2907–2926.
- Eickhoff SB, Bzdok D, Laird AR, Roski C, Caspers S, Zilles K, Fox PT (2011): Co-activation patterns distinguish cortical modules, their connectivity and functional differentiation. *Neuroimage* 57:938–949.
- Eickhoff SB, Bzdok D, Laird AR, Kurth F, Fox PT (2012): Activation likelihood estimation meta-analysis revisited. *Neuroimage* 59:2349–2361.
- Eickhoff SB, Thirion B, Varoquaux G, Bzdok D (2015): Connectivity-Based Parcellation: Critique and Implications. *Hum Brain Mapp* 36:4771–4792.
- Everitt BJ, Dickinson A, Robbins TW (2001): The neuropsychological basis of addictive behaviour. *Brain Res Brain Res Rev* 36:129–138.
- Fan L, Wang J, Zhang Y, Han W, Yu C, Jiang T (2014): Connectivity based parcellation of the human temporal pole using diffusion tensor imaging. *Cereb Cortex* 24:3365–3378.
- Fan L, Li H, Zhuo J, Zhang Y, Wang J, Chen L, Yang Z, Chu C, Xie S, Laird AR, Fox PT, Eickhoff SB, Yu C, Jiang T (2016): The human brainnetome atlas: A new brain atlas based on connective architecture. *Cereb Cortex* 26:3508–3526.
- Floresco SB (2015): The nucleus accumbens: An interface between cognition, emotion, and action. *Annu Rev Psychol* 66:25–52.
- Fornito A, Whittle S, Wood SJ, Velakoulis D, Pantelis C, Yucel M (2006): The influence of sulcal variability on morphometry of the human anterior cingulate and paracingulate cortex. *Neuroimage* 33:843–854.
- French SJ, Totterdell S (2003): Individual nucleus accumbens-projection neurons receive both basolateral amygdala and ventral subicular afferents in rats. *Neuroscience* 119:19–31.
- Gelfand Y, Kaplitt MG (2013): Gene therapy for psychiatric disorders. *World Neurosurg* 80:11–18.
- Genon S, Li H, Fan LZ, Muller VI, Gieslik EG, Hoffstaedter F, Reid AT, Langer R, Grefkes G, Fox PT, Moebus S, Gaspers S, Amunts K, Jiang TZ, Eickhoff SB (2017): The right dorsal premotor mosaic: Organization, functions, and connectivity. *Cereb Cortex* 27:2095–2110.
- Glasser MF, Sotiropoulos SN, Wilson JA, Coalson TS, Fischl B, Andersson JL, Xu J, Jbabdi S, Webster M, Polimeni JR, Van Essen DC, Jenkinson M (2013): The minimal preprocessing pipelines for the Human Connectome Project. *Neuroimage* 80:105–124.
- Groenewegen HJ, der Vermeulen-Van ZE, te KA, Witter MP (1987): Organization of the projections from the subiculum to the ventral striatum in the rat. A study using anterograde transport of Phaseolus vulgaris leucoagglutinin. *Neuroscience* 23:103–120.
- Groenewegen HJ, Wright CI, Beijer AV (1996): The nucleus accumbens: Gateway for limbic structures to reach the motor system? *Prog Brain Res* 107:485–511.
- Haber SN, Kunishio K, Mizobuchi M, Lynd-Balta E (1995): The orbital and medial prefrontal circuit through the primate basal ganglia. *J Neurosci* 15:4851–4867.
- Hardwick RM, Lesage E, Eickhoff CR, Clos M, Fox P, Eickhoff SB (2015): Multimodal connectivity of motor learning-related dorsal premotor cortex. *NeuroImage* 123:114–128.
- Heidbreder CA, Groenewegen HJ (2003): The medial prefrontal cortex in the rat: Evidence for a dorso-ventral distinction based upon functional and anatomical characteristics. *Neurosci Biobehav Rev* 27:555–579.
- Heimer L, Zahm DS, Churchill L, Kalivas PW, Wohltmann C (1991): Specificity in the projection patterns of accumbal core and shell in the rat. *Neuroscience* 41:89–125.
- Hoffstaedter F, Grefkes C, Caspers S, Roski C, Palomero-Gallagher N, Laird AR, Fox PT, Eickhoff SB (2014): The role of

- anterior midcingulate cortex in cognitive motor control: Evidence from functional connectivity analyses. *Hum Brain Mapp* 35:2741–2753.
- Humphries MD, Prescott TJ (2010): The ventral basal ganglia, a selection mechanism at the crossroads of space, strategy, and reward. *Prog Neurobiol* 90:385–417.
- Ikemoto K, Satoh K, Maeda T, Fibiger HC (1995): Neurochemical heterogeneity of the primate nucleus accumbens. *Exp Brain Res* 104:177–190.
- Ikemoto S (2007): Dopamine reward circuitry: Two projection systems from the ventral midbrain to the nucleus accumbens-olfactory tubercle complex. *Brain Res Rev* 56:27–78.
- Ito R, Robbins TW, Pennartz CM, Everitt BJ (2008): Functional interaction between the hippocampus and nucleus accumbens shell is necessary for the acquisition of appetitive spatial context conditioning. *J Neurosci* 28:6950–6959.
- Janssen RJ, Jylänki P, Kessels RPC, van Gerven MAJ (2015): Probabilistic model-based functional parcellation reveals a robust, fine-grained subdivision of the striatum. *NeuroImage* 119:398–405.
- Jbabdi S, Sotiropoulos SN, Savio AM, Grana M, Behrens TE (2012): Model-based analysis of multishell diffusion MR data for tractography: How to get over fitting problems. *Magn Reson Med* 68:1846–1855.
- Jenkinson M, Beckmann CF, Behrens TE, Woolrich MW, Smith SM (2012): FSL. *Neuroimage* 62:782–790.
- Johansen-Berg H, Behrens TE, Robson MD, Drobnjak I, Rushworth MF, Brady JM, Smith SM, Higham DJ, Matthews PM (2004): Changes in connectivity profiles define functionally distinct regions in human medial frontal cortex. *Proc Natl Acad Sci USA* 101:13335–13340.
- Kelly C, Uddin LQ, Shehzad Z, Margulies DS, Castellanos FX, Milham MP, Petrides M (2010): Broca's region: Linking human brain functional connectivity data and non-human primate tracing anatomy studies. *Eur J Neurosci* 32:383–398.
- Kelly C, Toro R, Di Martino A, Cox CL, Bellec P, Castellanos FX, Milham MP (2012): A convergent functional architecture of the insula emerges across imaging modalities. *Neuroimage* 61:1129–1142.
- Kringelbach ML, Rolls ET (2004): The functional neuroanatomy of the human orbitofrontal cortex: Evidence from neuroimaging and neuropsychology. *Prog Neurobiol* 72:341–372.
- Laird AR, Eickhoff SB, Kurth F, Fox PM, Uecker AM, Turner JA, Robinson JL, Lancaster JL, Fox PT (2009): ALE meta-analysis workflows via the brainmap database: Progress towards a probabilistic functional brain atlas. *Front Neuroinform* 3:23.
- Leonard CM, Towler S, Welcome S, Chiarello C (2009): Paracingulate asymmetry in anterior and midcingulate cortex: Sex differences and the effect of measurement technique. *Brain Struct Funct* 213:553–569.
- Liu H, Qin W, Li W, Fan L, Wang J, Jiang T, Yu C (2013): Connectivity-based parcellation of the human frontal pole with diffusion tensor imaging. *J Neurosci* 33:6782–6790.
- Lodge DJ, Grace AA (2006): The laterodorsal tegmentum is essential for burst firing of ventral tegmental area dopamine neurons. *Proc Natl Acad Sci USA* 103:5167–5172.
- Mannella F, Gurney K, Baldassarre G (2013): The nucleus accumbens as a nexus between values and goals in goal-directed behavior: A review and a new hypothesis. *Front Behav Neurosci* 7:135.
- Mars RB, Sallet J, Schuffelgen U, Jbabdi S, Toni I, Rushworth MF (2012): Connectivity-based subdivisions of the human right “temporoparietal junction area”: Evidence for different areas participating in different cortical networks. *Cereb Cortex* 22:1894–1903.
- Mars RB, Verhagen L, Gladwin TE, Neubert FX, Sallet J, Rushworth MF (2016): Comparing brains by matching connectivity profiles. *Neurosci Biobehav Rev* 60:90–97.
- Maurice N, Deniau JM, Glowinski J, Thierry AM (1999): Relationships between the prefrontal cortex and the basal ganglia in the rat: Physiology of the cortico-nigral circuits. *J Neurosci* 19:4674–4681.
- Mavridis I, Boviatsis E, Anagnostopoulou S (2011): Anatomy of the human nucleus accumbens: A combined morphometric study. *Surg Radiol Anat* 33:405–414.
- McCollum LA, Roberts RC (2014): Ultrastructural localization of tyrosine hydroxylase in tree shrew nucleus accumbens core and shell. *Neuroscience* 271:23–34.
- McCracken CB, Grace AA (2007): High-frequency deep brain stimulation of the nucleus accumbens region suppresses neuronal activity and selectively modulates afferent drive in rat orbitofrontal cortex in vivo. *J Neurosci* 27:12601–12610.
- Meilä M (2007): Comparing clusterings: An information based distance. *J Multivar Anal* 98:873–895.
- Moerel M, De Martino F, Formisano E (2014): An anatomical and functional topography of human auditory cortical areas. *Front Neurosci* 8:225.
- Mogenson GJ, Jones DL, Yim CY (1980): From motivation to action: Functional interface between the limbic system and the motor system. *Prog Neurobiol* 14:69–97.
- Murty VP, Shermohammed M, Smith DV, Carter RM, Huettel SA, Adcock RA (2014): Resting state networks distinguish human ventral tegmental area from substantia nigra. *Neuroimage* 100:580–589.
- Napadow V, Dhond R, Kennedy D, Hui KK, Makris N (2006): Automated brainstem co-registration (ABC) for MRI. *Neuroimage* 32:1113–1119.
- Neto LL, Oliveira E, Correia F, Ferreira AG (2008): The human nucleus accumbens: Where is it? A stereotactic, anatomical and magnetic resonance imaging study. *Neuromodulation* 11:13–22.
- Neubert FX, Mars RB, Thomas AG, Sallet J, Rushworth MF (2014): Comparison of human ventral frontal cortex areas for cognitive control and language with areas in monkey frontal cortex. *Neuron* 81:700–713.
- Nichols T, Brett M, Andersson J, Wager T, Poline JB (2005): Valid conjunction inference with the minimum statistic. *Neuroimage* 25:653–660.
- Nicola SM (2007): The nucleus accumbens as part of a basal ganglia action selection circuit. *Psychopharmacology (Berl)* 191:521–550.
- Parkinson JA, Willoughby PJ, Robbins TW, Everitt BJ (2000): Disconnection of the anterior cingulate cortex and nucleus accumbens core impairs Pavlovian approach behavior: Further evidence for limbic cortical-ventral striatopallidal systems. *Behav Neurosci* 114:42–63.
- Passingham RE, Stephan KE, Kötter R (2002): The anatomical basis of functional localization in the cortex. *Nat Rev Neurosci* 3:606–616.
- Patenaude B, Smith SM, Kennedy DN, Jenkinson M (2011): A Bayesian model of shape and appearance for subcortical brain segmentation. *Neuroimage* 56:907–922.
- Paus T (2001): Primate anterior cingulate cortex: Where motor control, drive and cognition interface. *Nat Rev Neurosci* 2:417–424.



- Pecina S, Berridge KC (2005): Hedonic hot spot in nucleus accumbens shell: Where do mu-opioids cause increased hedonic impact of sweetness? *J Neurosci* 25:11777–11786.
- Peters J, LaLumiere RT, Kalivas PW (2008): Infralimbic prefrontal cortex is responsible for inhibiting cocaine seeking in extinguished rats. *J Neurosci* 28:6046–6053.
- Ray KL, Zald DH, Bludau S, Riedel MC, Bzdok D, Yanes J, Falcone KE, Amunts K, Fox PT, Eickhoff SB, Laird AR (2015): Co-activation based parcellation of the human frontal pole. *Neuroimage* 123:200–211.
- Reed MD, Hildebrand DG, Santangelo G, Moffa A, Pira AS, Rycyna L, Radic M, Price K, Archbold J, McConnell K, Girard L, Morin K, Tang A, Febo M, Stellar JR (2015): Assessing contributions of nucleus accumbens shell subregions to reward-seeking behavior. *Drug Alcohol Depend* 153:369–373.
- Reid AT, Bzdok D, Langner R, Fox PT, Laird AR, Amunts K, Eickhoff SB, Eickhoff CR (2016): Multimodal connectivity mapping of the human left anterior and posterior lateral prefrontal cortex. *Brain Struct Funct* 221:2589–2605.
- Rigoard P, Buffenoir K, Jaafari N, Giot JP, Houeto JL, Mertens P, Velut S, Bataille B (2011): The accumbofrontal fasciculus in the human brain: A microsurgical anatomical study. *Neurosurgery* 68:1102–1111.
- Robinson JL, Laird AR, Glahn DC, Lovallo WR, Fox PT (2010): Metaanalytic connectivity modeling: Delineating the functional connectivity of the human amygdala. *Hum Brain Mapp* 31:173–184.
- Roesch MR, Calu DJ, Schoenbaum G (2007): Dopamine neurons encode the better option in rats deciding between differently delayed or sized rewards. *Nat Neurosci* 10:1615–1624.
- Salgado S, Kaplitt MG (2015): The nucleus accumbens: A comprehensive review. *Stereotact Funct Neurosurg* 93:75–93.
- Saunders BT, Robinson TE (2012): The role of dopamine in the accumbens core in the expression of Pavlovian-conditioned responses. *Eur J Neurosci* 36:2521–2532.
- Seibert TM, Brewer JB (2011): Default network correlations analyzed on native surfaces. *J Neurosci Methods* 198:301–311.
- Sesia T, Temel Y, Lim L, Blokland A, Steinbusch HW, Visser-Vandewalle V (2008): Deep brain stimulation of the nucleus accumbens core and shell: Opposite effects on impulsive action. *Exp Neurol* 214:135–139.
- Smith SM, Beckmann CF, Andersson J, Auerbach EJ, Bijsterbosch J, Douaud G, Duff E, Feinberg DA, Griffanti L, Harms MP, Kelly M, Laumann T, Miller KL, Moeller S, Petersen S, Power J, Salimi-Khorshidi G, Snyder AZ, Vu AT, Woolrich MW, Xu J, Yacoub E, Ugurbil K, Van Essen DC, Glasser MF (2013): Resting-state fMRI in the Human Connectome Project. *Neuroimage* 80:144–168.
- Sotiropoulos SN, Jbabdi S, Xu J, Andersson JL, Moeller S, Auerbach EJ, Glasser MF, Hernandez M, Sapiro G, Jenkinson M, Feinberg DA, Yacoub E, Lenglet C, Van Essen DC, Ugurbil K, Behrens TE (2013): Advances in diffusion MRI acquisition and processing in the Human Connectome Project. *Neuroimage* 80:125–143.
- Sporns O, Tononi G, Kotter R (2005): The human connectome: A structural description of the human brain. *PLoS Comput Biol* 1:e42.
- Stopper CM, Floresco SB (2011): Contributions of the nucleus accumbens and its subregions to different aspects of risk-based decision making. *Cogn Affect Behav Neurosci* 11:97–112.
- Sturm V, Lenartz D, Koulousakis A, Treuer H, Herholz K, Klein JC, Klosterkötter J (2003): The nucleus accumbens: A target for deep brain stimulation in obsessive-compulsive- and anxiety-disorders. *J Chem Neuroanat* 26:293–299.
- Thirion B, Varoquaux G, Dohmatob E, Poline JB (2014): Which fMRI clustering gives good brain parcellations? *Front Neurosci* 8:167.
- Turkeltaub PE, Eickhoff SB, Laird AR, Fox M, Wiener M, Fox P (2012): Minimizing within-experiment and within-group effects in activation likelihood estimation meta-analyses. *Hum Brain Mapp* 33:1–13.
- Tziortzi AC, Haber SN, Searle GE, Tsoumpas C, Long CJ, Shotbolt P, Douaud G, Jbabdi S, Behrens TEJ, Rabiner EA, Jenkinson M, Gunn RN (2013): Connectivity-based functional analysis of dopamine release in the striatum using diffusion-weighted MRI and positron emission tomography. *Cereb Cortex* 24:1165–1177.
- Ugurbil K, Xu J, Auerbach EJ, Moeller S, Vu AT, Duarte-Carvajalino JM, Lenglet C, Wu X, Schmitter S, Van de Moortele PF, Strupp J, Sapiro G, De Martino F, Wang D, Harel N, Garwood M, Chen L, Feinberg DA, Smith SM, Miller KL, Sotiropoulos SN, Jbabdi S, Andersson JL, Behrens TE, Glasser MF, Van Essen DC, Yacoub E (2013): Pushing spatial and temporal resolution for functional and diffusion MRI in the Human Connectome Project. *Neuroimage* 80:80–104.
- van den Heuvel MP, Scholtens LH, Feldman Barrett L, Hilgetag CC, de Reus MA (2015): Bridging cytoarchitectonics and connectomics in human cerebral cortex. *J Neurosci* 35:13943–13948.
- Van der Werf YD, Witter MP, Groenewegen HJ (2002): The intralaminar and midline nuclei of the thalamus. Anatomical and functional evidence for participation in processes of arousal and awareness. *Brain Res Brain Res Rev* 39:107–140.
- van Dongen YC, Deniau JM, Pennartz CM, Galis-de GY, Voorn P, Thierry AM, Groenewegen HJ (2005): Anatomical evidence for direct connections between the shell and core subregions of the rat nucleus accumbens. *Neuroscience* 136:1049–1071.
- Van Essen DC, Smith SM, Barch DM, Behrens TE, Yacoub E, Ugurbil K (2013): The WU-Minn Human Connectome Project: An overview. *Neuroimage* 80:62–79.
- Volkow ND, Morales M (2015): The brain on drugs: From reward to addiction. *Cell* 162:712–725.
- Voorn P, Brady LS, Berendse HW, Richfield EK (1996): Densitometrical analysis of opioid receptor ligand binding in the human striatum: I. Distribution of opioid receptor defines shell and core of the ventral striatum. *Neuroscience* 75:777–792.
- Voorn P, Vanderschuren LJ, Groenewegen HJ, Robbins TW, Pennartz CM (2004): Putting a spin on the dorsal-ventral divide of the striatum. *Trends Neurosci* 27:468–474.
- Wang J, Fan L, Zhang Y, Liu Y, Jiang D, Zhang Y, Yu C, Jiang T (2012): Tractography-based parcellation of the human left inferior parietal lobule. *NeuroImage* 63:641–652.
- Wang J, Yang Y, Fan L, Xu J, Li C, Liu Y, Fox PT, Eickhoff SB, Yu C, Jiang T (2015): Convergent functional architecture of the superior parietal lobule unraveled with multimodal neuroimaging approaches. *Hum Brain Mapp* 36:238–257.
- Wang J, Zhang J, Rong M, Wei X, Zheng D, Fox PT, Eickhoff SB, Jiang T (2016): Functional topography of the right inferior parietal lobule structured by anatomical connectivity profiles. *Hum Brain Mapp* 12:4316–4332.
- Wang SF, Ritchey M, Libby LA, Ranganath C (2016): Functional connectivity based parcellation of the human medial temporal lobe. *Neurobiol Learn Mem* 134:123–134.
- Wright CI, Groenewegen HJ (1996): Patterns of overlap and segregation between insular cortical, intermediodorsal thalamic and basal amygdaloid afferents in the nucleus accumbens of the rat. *Neuroscience* 73:359–373.



- Yamaguchi T, Goto A, Nakahara I, Yawata S, Hikida T, Matsuda M, Funabiki K, Nakanishi S (2015): Role of PKA signaling in D2 receptor-expressing neurons in the core of the nucleus accumbens in aversive learning. *Proc Natl Acad Sci USA* 112:11383–11388.
- Zaborszky L, Alheid GF, Beinfeld MC, Eiden LE, Heimer L, Palkovits M (1985): Cholecystokinin innervation of the ventral striatum: A morphological and radioimmunological study. *Neuroscience* 14:427–453.
- Zahm DS (1999): Functional-anatomical implications of the nucleus accumbens core and shell subterritories. *Ann N Y Acad Sci* 877:113–128.
- Zahm DS, Brog JS (1992): On the significance of subterritories in the “accumbens” part of the rat ventral striatum. *Neuroscience* 50:751–767.
- Zahm DS, Heimer L (1993): Specificity in the efferent projections of the nucleus accumbens in the rat: Comparison of the rostral pole projection patterns with those of the core and shell. *J Comp Neurol* 327:220–232.
- Zhang Y, Brady M, Smith S (2001): Segmentation of brain MR images through a hidden Markov random field model and the expectation-maximization algorithm. *IEEE Trans Med Imaging* 20:45–57.
- Zhu Y, Wienecke CF, Nachtrab G, Chen X (2016): A thalamic input to the nucleus accumbens mediates opiate dependence. *Nature* 530:219–222.
- Zuo XN, Di Martino A, Kelly C, Shehzad ZE, Gee DG, Klein DF, Castellanos FX, Biswal BB, Milham MP (2010): The oscillating brain: Complex and reliable. *Neuroimage* 49:1432–1445.